Electronic Supplementary Material (ESI) for Inorganic Chemistry Frontiers.
This journal is © the Partner Organisations 2022

Supporting Information for the Article

Towards Determining Molecular Structure with ESI-MS Backed by Computational Methods: Structures of Subnanoclusters of Pd and Cu Chlorides, Ion Dynamics in Vacuum, and Challenges to the Methodology

Anton A. Bondarenko†, Yulia S. Vlasova‡§, Mikhail V. Polynski†‡§,*

Valentina V. Ilyushenkova‡, Valentine P. Ananikov†‡§*

† Saint Petersburg State University, Universitetsky Prospect 26, Saint Petersburg 198504, Russia.

‡ Zelinsky Institute of Organic Chemistry, Russian Academy of Sciences, Leninsky Prospect 47, Moscow 119991, Russia.

§ MSU, Faculty of Chemistry, Leninskiye Gory 1-3, Moscow 119991, Russia

* polynskimikhail@gmail.com (M.V.P.); val@ioc.ac.ru (V.P.A.).

Table of Contents

1. The MSARIS Package

The MSARIS package comprises several scripts that can be used to analyze mass spectrometry data. In this study, we applied MSARIS within a unified workflow to identify ions in spectra. This workflow consists of several separate stages. Among the former, the ProteoWizard package was applied to interpret and convert files from proprietary Bruker format to mzML. Converting a spectrum into open mzML format allows performing analysis by using packages written in Python, which were used in our workflow.

MSARIS combines some packages from OpenMS with its Python 3 API together with signal processing functions and classes available in SciPy and IsoSpec. The latter was used to calculate isotopic distributions and estimate weighted masses of ions in spectra. Calculated weighted masses were selected as target parameters in optimization with the `pulp` package by applying the default solver. The optimization was performed to obtain ion formulae by finding an optimal integer solution to a set of predefined linear equations and inequalities. The linear equations and inequalities expressed heuristic rules of valency, charge, and mass conservation. Additionally, the heuristics constrained the possible fraction of impurities (as O_2, N_2, H_2O, etc.) and metal ions that underwent reduction or oxidation. In such a way, for every calculated ionic mass in a spectrum, a set of potential molecular formulae were generated. The obtained formulae were used to calculate isotopomeric *m*/*z* and intensities by generating isotope distributions with the IsoSpec package and, consequentially, by simulating spectra from the generated distributions. Generated spectra are compared with the experimental spectra after filtering by the cos_dist metric (see below).

The MSARIS package contains several three groups of scripts applied consequentially (Figure S1):

1. Loading and preprocessing of MS data;
2. Finding isotopic pattern clusters (isotopomers of ions) and calculating weighted masses of ions;
3. Determining ion formulae with linear optimization.

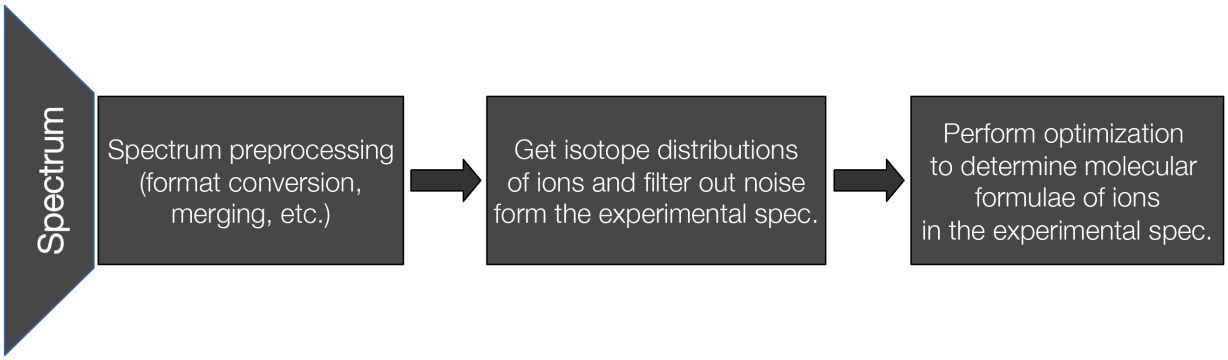

Figure S1. Three consequential stages of MS data analysis with MSARIS.

1.1.Details of Data Analysis with MSARIS

The workflow chart in Figure S2a illustrates the algorithm in more detail. The spectrum loading and preprocessing were conducted using functions and classes available in the OpenMS package. The data loading was followed by data filtration using a relative threshold equal to 1/1000 of a highest peak intensity. Then, we applied the SpecraMerger function from the OpenMS framework to merge spectra from individual scans and increase the S/N ratio. Finally, peaks below the relative intensity of 1% were filtered out as noise. After that, relative intensities were calculated in merged

spectra (one merged spectrum per ESI-MS experiment). For every solution, we performed three ESI-MS experiments. Intensities presented in processed spectra in the main text are mean values averaged over three experiments. Error bars represent the unbiased standard error of the mean computed with `pandas.DataFrame.sem`.

Then, we searched for clusters of isotopomer signals and calculated the molecular masses of ions. The algorithm of cluster search is depicted in Figure S2b. The clusterization is based on selecting a locally maximal peak and the predefined spectral window defined in the vicinity of a maximal peak. A Python class for clustering MaxClustering accepts as an initialization parameter a window width for a cluster and a threshold to sort out noise. In this article, 0.1% relative intensity (from maximal peak intensity) was used as a threshold to select only relevant and stable signals. The selection of spectral windows, including clusters of isotopomers, was iteratively performed until no peaks were left. As a result, a data structure based on a Python dictionary was formed. The dictionaries had keys equal to weighted ion masses and mass spectra as dictionary values (see Figure S2b).

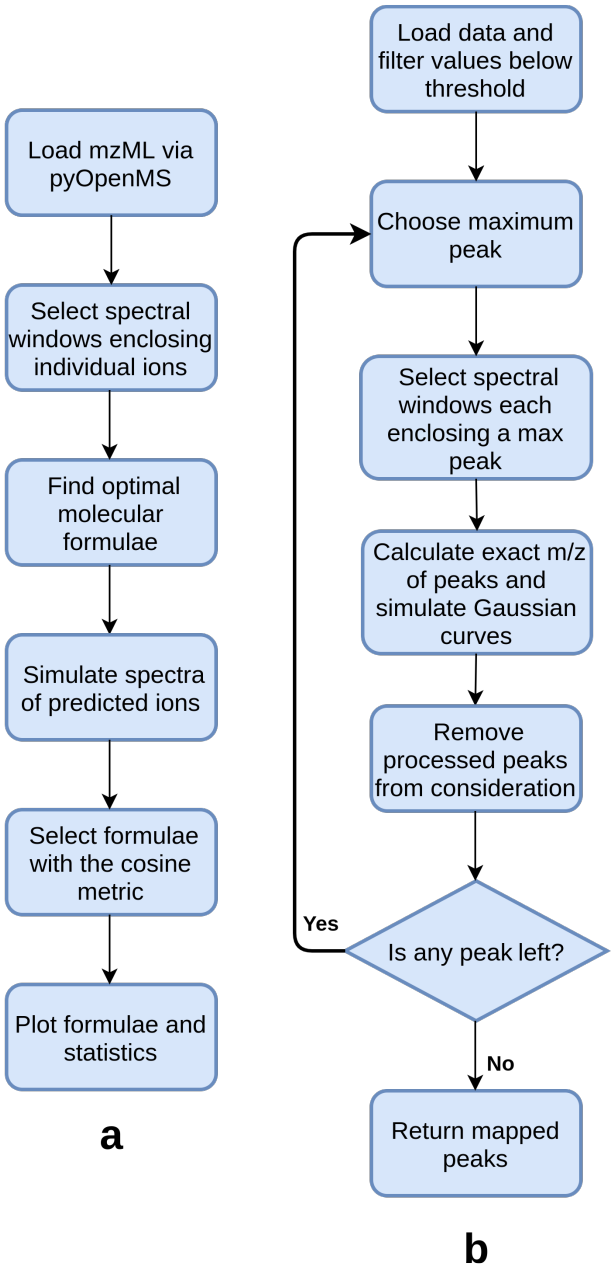

Figure S2. The main workflow and algorithms for clustering and calculating optimal ion formulae: a) general workflow of the process aimed to identify signals in a mass spectrum; b) algorithm of MaxCluster to select signals of individual ions in filtered spectra.

In our case, overlapping series of peaks were rarely present. Therefore, by filtering and adjusting window parameters for selected peak series, we could separate signals of individual ions in spectra. After finding a spectral window enclosing isotopomers of a given ion, ion molecular mass was calculated as a weighted sum of *m*/*z*.

The weighed masses were used as target quantities in searching for an ion molecular formula via optimization with the `pulp` package. The molecular formula was determined as the optimal integer solution (coefficients in the molecular formula) within a predefined tolerance of a set of linear equations and inequalities.

The cosine metric is commonly used to estimate the similarity of multidimensional vectors. Previous studies have demonstrated the application of the cos_dist metric to assess theoretical and experimental spectra.[1] We used the SciPy package to calculate cos_dist according to the following formula:

$$\text{cos\_dist}(\text{u}, \text{v}) = 1 - \frac{u \cdot v}{\|u\| \|v\|},$$

Where u and v are vectors consisting of *m*/*z* and normalized relative intensities of theoretical and experimental spectra. In such a way, the cos_dist metric compares not only *m*/*z* of theoretical and experimental spectra, but also isotope patterns. Given the fact that the considered transition metals produce distinct isotope patterns, the use of the cos_dist metric seem especially efficient for transition metal systems.

Optimizations for each ligand (excluding the TBA^+ ion) from Table S1 were performed separately in the epsilon range (tolerance) starting from 5 *m*/*z* with step 0.1. The initial molecular formulae found in optimization were filtered using the cos_dist metric equal to 0.5. To ensure that cos_dist correctly estimates spectra, we applied a heuristic by cutting from original peaks in a window of approximately 0.1 *m*/*z* around theoretical signals. Such a technique ensured that we

compare signals without noise and decrease interference. A stepwise increase in optimization tolerance allowed us to overcome the imperfect accuracy of clusterization algorithms caused by overlapping signals of impurities present in some spectral windows for relevant ions.

MSARIS calculations resulted in several potential molecular formulae for many complex ions of relatively high molecular weight. Hence, filtering by cos_dist similarity was applied to find correct formulae with the lowest value of the metric. Furthermore, an aggregation of three separate experiments allowed us to identify only statistically significant signals (omnipresent in all three experiments) and eliminated erroneous formula candidates that can be related to algorithmic noise.

Table S1. Molar weights of transition metals, cations, anions, and neutral ligands used in the optimization based on the molecular fragment approach.

Name	Mass	Charge
Pd1	106.4200	+1
Pd2	106.4200	+2
Cu1	63.5460	+1
Cu2	63.5460	+2
Na	22.9898	+1
K	39.0983	+1
TBA	242.2842	+1
OH	17.0033	-1
Cl	35.4500	-1
Br	79.9040	-1

CF3COO	112.9856	-1
O2_1	31.9898	-1
O2_2	31.9898	-2
O	15.99903	-2
CH3CN	41.0265	0
CH3OH	32.0262	0
N2	28.0061	0
H2O	18.0106	0

2. Simulating and Plotting Realistic ESI-MS Spectra and Plotting Experimental Data

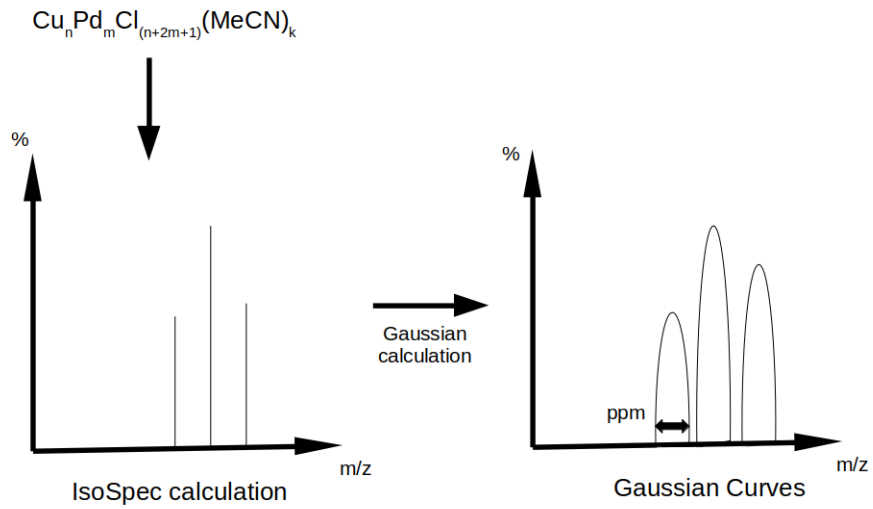

Figure S3. Simulating an MS spectrum by using an isotope distribution calculated with IsoSpec.

Figure S3 depicts the main stages of spectrum simulation in our implementation. IsoSpec was used to calculate theoretical isotope distributions. Next, isotopomer signals are simulated as Gaussians, in which the half-width parameter (σ of the Gaussian distribution) is defined in ppm and based on the FMWH calculation (see below), which allows fine-tuning the width of the peaks.

Our initial testing runs demonstrated that isotope pattern calculation is the most time-consuming part of the optimization described below. To speed up calculations, an option to save previously calculated patterns was implemented. Testing showed that the save feature significantly accelerated the simulations of the MS spectra of ions.

MS spectra of individual ions (both predicted and cut off from an original spectrum) can be visualized by using the Matplotlib package in the form of an isotope overlay, as well as a total experimental spectrum with marked successfully assigned peaks. Furthermore, tables demonstrating candidates and their deviation metrics can be constructed automatically. All

MSARIS predictions were compared with our conventional manual analysis of the obtained ESI-MS spectra.

2.1. Spectra Simulation Algorithm in Detail

IsoSpec[2,3] is a fine isotopic structure calculator software that generates a list of high-precision masses m_i of isotopomers with corresponding calculated p_i probabilities of occurrences for a given molecular formula. To simulate a realistic mass spectrum, one would need to extrapolate a set of (m_i, p_i) with a continuous function.[4] It was achieved by convolution. Mathematically, such spike trains, sets of (m_i, p_i), can be represented as a sum of Dirac delta functions scaled by probability coefficient:[5]

$$p(m) = \sum_i \delta(m - m_i) \cdot p_i.$$

Each spike train can be transformed into a continuous function via convolution with a smoothing function $h(m)$:

$$f_p(m) = ph = \sum_i h(m - m_i).$$

The smoothing function was chosen to be the Gaussian function:

$$h(m) = \frac{1}{\sigma\sqrt{2\pi}} e^{-\frac{m^2}{2\sigma^2}},$$

where m_i is the mass of isotopomer, and σ represents the spectral resolution through full width at high maximum FWHM variable (FWHM), so:

$$\sigma = \frac{FWHM}{2\sqrt{2\ln(2)}},$$

where

$$FWHM = \frac{ppm}{10^6} m_i.$$

3. Figures: PEG Signals

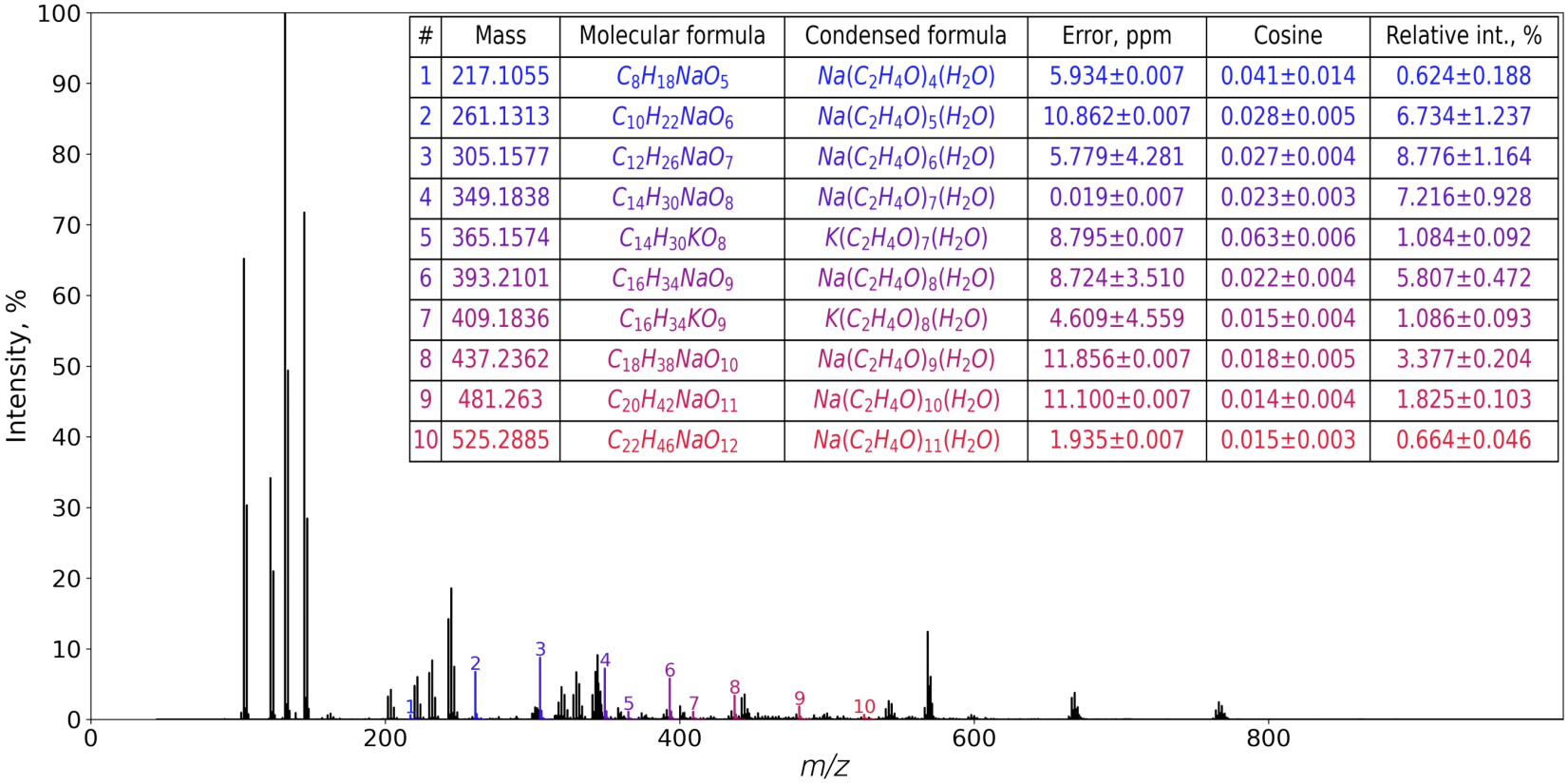

#	Mass	Molecular formula	Condensed formula	Error, ppm	Cosine	Relative int., %
1	217.1055	$C_8H_{18}NaO_5$	$Na(C_2H_4O)_4(H_2O)$	5.934±0.007	0.041±0.014	0.624±0.188
2	261.1313	$C_{10}H_{22}NaO_6$	$Na(C_2H_4O)_5(H_2O)$	10.862±0.007	0.028±0.005	6.734±1.237
3	305.1577	$C_{12}H_{26}NaO_7$	$Na(C_2H_4O)_6(H_2O)$	5.779±4.281	0.027±0.004	8.776±1.164
4	349.1838	$C_{14}H_{30}NaO_8$	$Na(C_2H_4O)_7(H_2O)$	0.019±0.007	0.023±0.003	7.216±0.928
5	365.1574	$C_{14}H_{30}KO_8$	$K(C_2H_4O)_7(H_2O)$	8.795±0.007	0.063±0.006	1.084±0.092
6	393.2101	$C_{16}H_{34}NaO_9$	$Na(C_2H_4O)_8(H_2O)$	8.724±3.510	0.022±0.004	5.807±0.472
7	409.1836	$C_{16}H_{34}KO_9$	$K(C_2H_4O)_8(H_2O)$	4.609±4.559	0.015±0.004	1.086±0.093
8	437.2362	$C_{18}H_{38}NaO_{10}$	$Na(C_2H_4O)_9(H_2O)$	11.856±0.007	0.018±0.005	3.377±0.204
9	481.263	$C_{20}H_{42}NaO_{11}$	$Na(C_2H_4O)_{10}(H_2O)$	11.100±0.007	0.014±0.004	1.825±0.103
10	525.2885	$C_{22}H_{46}NaO_{12}$	$Na(C_2H_4O)_{11}(H_2O)$	1.935±0.007	0.015±0.003	0.664±0.046

Figure S4. PEG impurity signals in the spectrum of CuCl solution (positive mode). Mass measurement errors (fourth columns in the inset table) were calculated according to the well-known formula.[6]

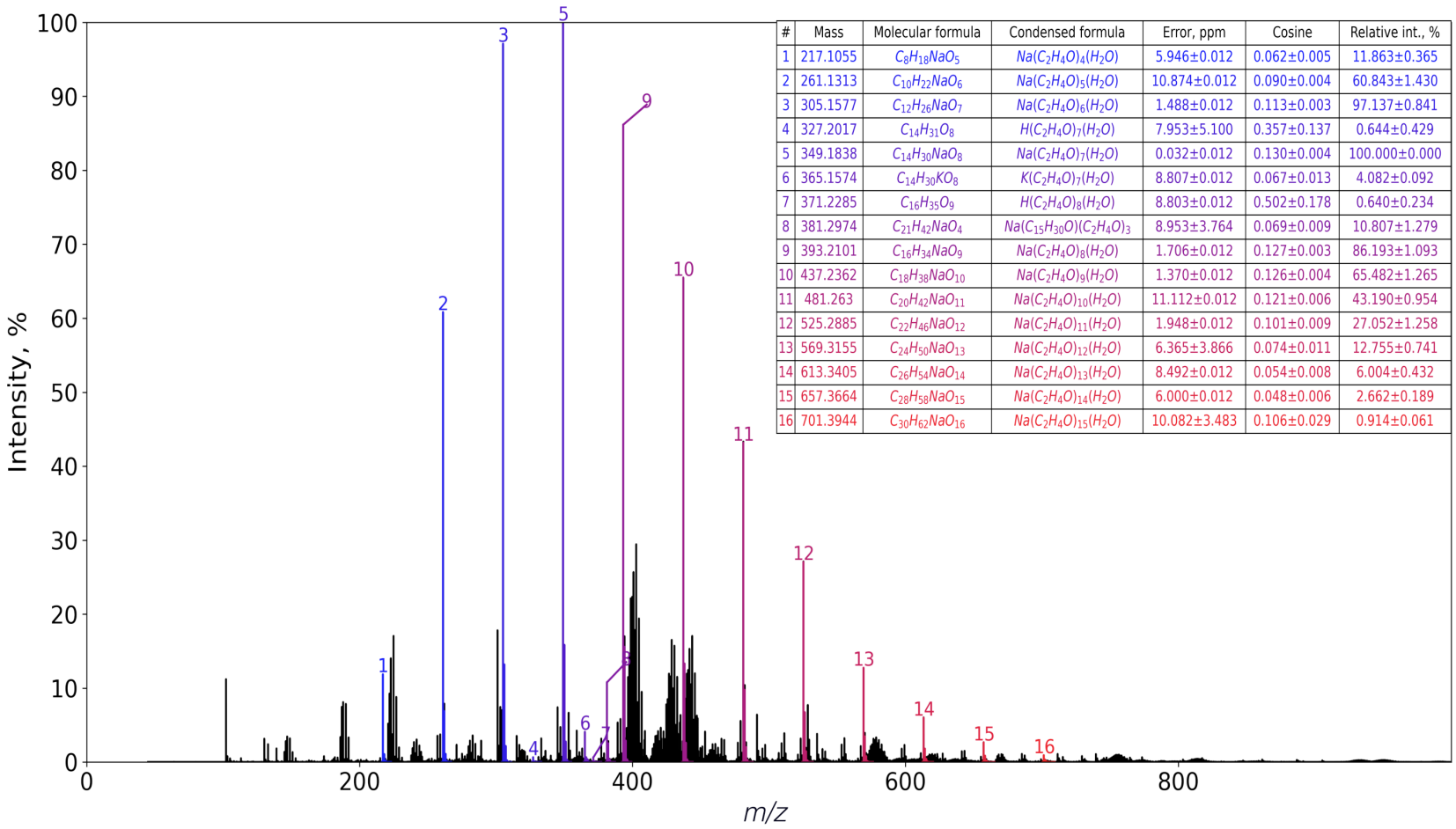

#	Mass	Molecular formula	Condensed formula	Error, ppm	Cosine	Relative int., %
1	217.1055	$C_8H_{18}NaO_5$	$Na(C_2H_4O)_4(H_2O)$	5.946±0.012	0.062±0.005	11.863±0.365
2	261.1313	$C_{10}H_{22}NaO_6$	$Na(C_2H_4O)_5(H_2O)$	10.874±0.012	0.090±0.004	60.843±1.430
3	305.1577	$C_{12}H_{26}NaO_7$	$Na(C_2H_4O)_6(H_2O)$	1.488±0.012	0.113±0.003	97.137±0.841
4	327.2017	$C_{14}H_{31}O_8$	$H(C_2H_4O)_7(H_2O)$	7.953±5.100	0.357±0.137	0.644±0.429
5	349.1838	$C_{14}H_{30}NaO_8$	$Na(C_2H_4O)_7(H_2O)$	0.032±0.012	0.130±0.004	100.000±0.000
6	365.1574	$C_{14}H_{30}KO_8$	$K(C_2H_4O)_7(H_2O)$	8.807±0.012	0.067±0.013	4.082±0.092
7	371.2285	$C_{16}H_{35}O_9$	$H(C_2H_4O)_8(H_2O)$	8.803±0.012	0.502±0.178	0.640±0.234
8	381.2974	$C_{21}H_{42}NaO_4$	$Na(C_{15}H_{30}O)(C_2H_4O)_3$	8.953±3.764	0.069±0.009	10.807±1.279
9	393.2101	$C_{16}H_{34}NaO_9$	$Na(C_2H_4O)_8(H_2O)$	1.706±0.012	0.127±0.003	86.193±1.093
10	437.2362	$C_{18}H_{38}NaO_{10}$	$Na(C_2H_4O)_9(H_2O)$	1.370±0.012	0.126±0.004	65.482±1.265
11	481.263	$C_{20}H_{42}NaO_{11}$	$Na(C_2H_4O)_{10}(H_2O)$	11.112±0.012	0.121±0.006	43.190±0.954
12	525.2885	$C_{22}H_{46}NaO_{12}$	$Na(C_2H_4O)_{11}(H_2O)$	1.948±0.012	0.101±0.009	27.052±1.258
13	569.3155	$C_{24}H_{50}NaO_{13}$	$Na(C_2H_4O)_{12}(H_2O)$	6.365±3.866	0.074±0.011	12.755±0.741
14	613.3405	$C_{26}H_{54}NaO_{14}$	$Na(C_2H_4O)_{13}(H_2O)$	8.492±0.012	0.054±0.008	6.004±0.432
15	657.3664	$C_{28}H_{58}NaO_{15}$	$Na(C_2H_4O)_{14}(H_2O)$	6.000±0.012	0.048±0.006	2.662±0.189
16	701.3944	$C_{30}H_{62}NaO_{16}$	$Na(C_2H_4O)_{15}(H_2O)$	10.082±3.483	0.106±0.029	0.914±0.061

Figure S5. PEG impurity signals in the spectrum of $PdCl_2$ solution (positive mode).

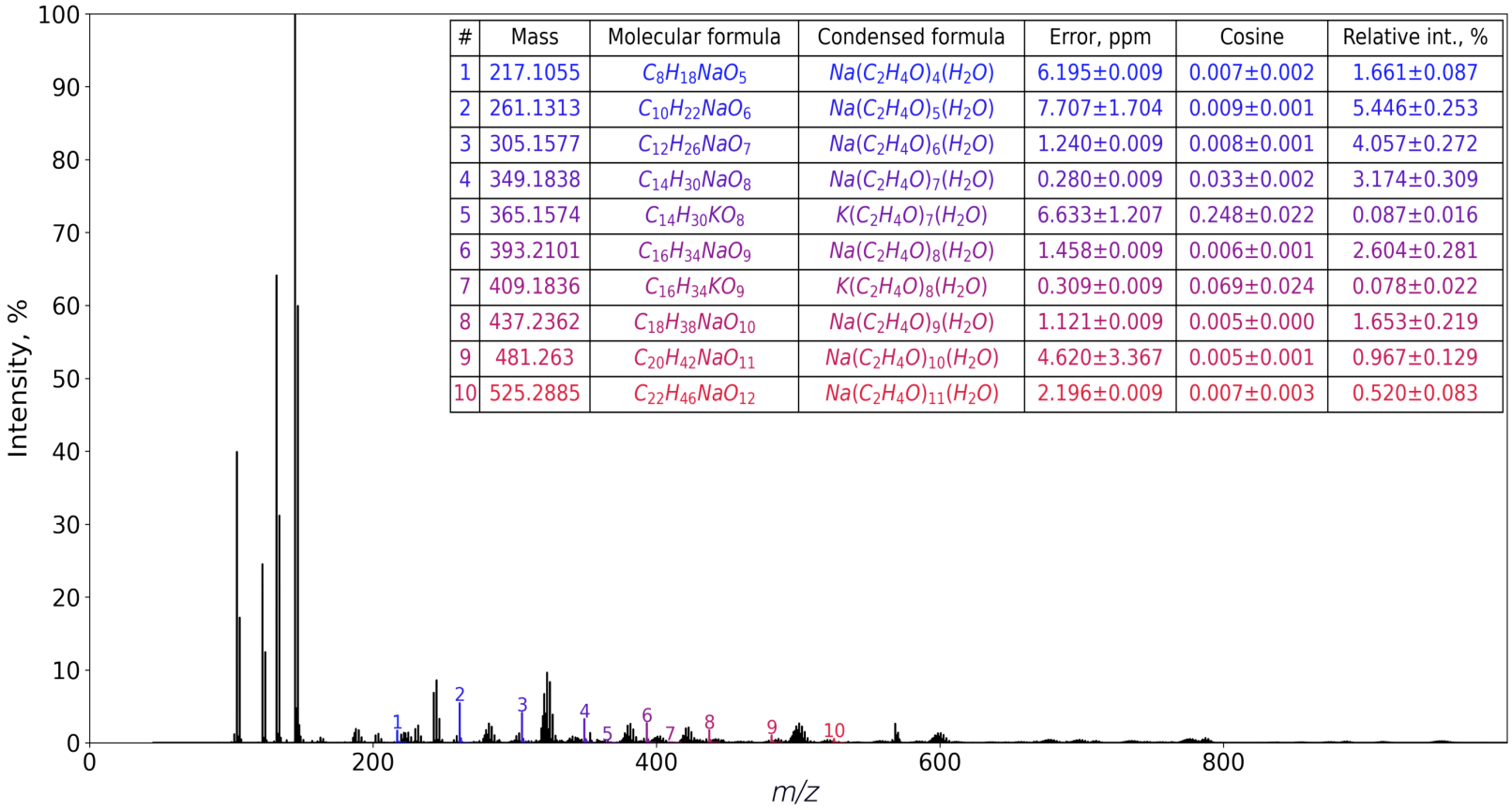

#	Mass	Molecular formula	Condensed formula	Error, ppm	Cosine	Relative int., %
1	217.1055	$C_8H_{18}NaO_5$	$Na(C_2H_4O)_4(H_2O)$	6.195±0.009	0.007±0.002	1.661±0.087
2	261.1313	$C_{10}H_{22}NaO_6$	$Na(C_2H_4O)_5(H_2O)$	7.707±1.704	0.009±0.001	5.446±0.253
3	305.1577	$C_{12}H_{26}NaO_7$	$Na(C_2H_4O)_6(H_2O)$	1.240±0.009	0.008±0.001	4.057±0.272
4	349.1838	$C_{14}H_{30}NaO_8$	$Na(C_2H_4O)_7(H_2O)$	0.280±0.009	0.033±0.002	3.174±0.309
5	365.1574	$C_{14}H_{30}KO_8$	$K(C_2H_4O)_7(H_2O)$	6.633±1.207	0.248±0.022	0.087±0.016
6	393.2101	$C_{16}H_{34}NaO_9$	$Na(C_2H_4O)_8(H_2O)$	1.458±0.009	0.006±0.001	2.604±0.281
7	409.1836	$C_{16}H_{34}KO_9$	$K(C_2H_4O)_8(H_2O)$	0.309±0.009	0.069±0.024	0.078±0.022
8	437.2362	$C_{18}H_{38}NaO_{10}$	$Na(C_2H_4O)_9(H_2O)$	1.121±0.009	0.005±0.000	1.653±0.219
9	481.263	$C_{20}H_{42}NaO_{11}$	$Na(C_2H_4O)_{10}(H_2O)$	4.620±3.367	0.005±0.001	0.967±0.129
10	525.2885	$C_{22}H_{46}NaO_{12}$	$Na(C_2H_4O)_{11}(H_2O)$	2.196±0.009	0.007±0.003	0.520±0.083

Figure S6. PEG impurity signals in the spectrum of the $PdCl_2$ and CuCl solution mixture (positive mode).

4. Quantum Chemical Calculations: Computational Details

The original `xtb` code (version 6.3.3)[7] was used to simulate molecular dynamics (MD) and perform metadynamics (MetaD) runs[8] with the GFN2-xTB Hamiltonian.[9] Additionally, pre-MD and pre-MetaD optimizations. 50 ps were simulated in all runs, and NVT conditions were selected (T = 398.15 K in the MetaD runs, and T = 473.15 K in MD runs). Molecular geometries in XYZ format were written to the trajectories every 20 fs. Each ps of MetaD runs, a molecular geometry was saved to subsequent geometry optimization and energy-based filtering (49 structures per trajectory, see below). The standard time step of 0.5 fs was selected, and no constraints on atom vibrations were imposed. The "sccacc" parameter was set to 1.0. All systems in MD and MetaD runs were confined in a spherically symmetrical cavity encompassing all atoms by applying the "logfermi" potential with a radial parameter equal to 37.8 Bohr radii. The "kpush" and "alp" parameters in the MetaD runs were set equal to 0.02 and 0.01, respectively, which allowed gradual sampling of isomer structures on picosecond time scales and resulted in the dissociation of ions after possible isomer structures were sampled.

Post-MetaD optimizations of sampled structures (49 structures per trajectory) were performed in ORCA 4.2.1.[10] All optimizations were followed by normal mode analysis (at T = 473.15 K). Vibrational frequencies were calculated via the finite differences procedure ("NUMFREQ").

Molecules were sorted with the following energy function U:

$$U = E_{el} + E_{ZPVE} + U_{vib} \qquad (1),$$

where E_{el} is the molecular "electronic" energy (all empirical corrections included), E_{ZPVE} is the molecular zero-point vibrational energy, and U_{vib} is the molecular inner energy in harmonic approximation at T = 473.15 K. U is basically molecular internal energy with contributions from rotational and translational motions neglected. As long as molecular rotational (U_{rot}) and

translational motion (U_{trans}) in the chamber of a TOF mass analyzer is not free but governed by an electric field of predefined potential, we neglected U_{rot} and U_{trans} in Equation (1). In this case, including the effect of a uniform electric field on molecular energy would be desirable; however, such a feature does not seem to be implemented in the program yet.

The so-defined inner energy U was used to sort and select ions. Ions obtained by structural sampling in MetaD runs followed by geometry optimization differing by less than 0.1 kcal/mol in U were considered as identical. Any structures (isomers, conformers, and transition states) having U greater than 10 kcal/mol relative to the lowest-U structure were neglected. Only minima on the PES were selected for further consideration (TS structures were neglected). The default geometry optimization procedure implemented in ORCA 4.2.1 for GFN2-xTB with the "TightOpt" convergence criterion was enough to obtain structures without any imaginary modes in the NUMFREQ procedure (Hessian calculation using the finite difference method) in all cases except one, $[Cu_3Cl_2(CH_3CN)(N_2)]^+$ (iso1). In the latter case we had to use the original `xtb` code with the "--opt extreme" option; after this optimization of geometry resulted in a structure which had no imaginary modes according to the NUMFREQ procedure performed in ORCA 4.2.1.

Such a procedure for isomer selection could lead to a situation when energetically degenerate isomers are filtered out, as, for example, can happen for enantiomers. We are not interested in such a case yet. For simplicity, we used the approach described above. Additionally, some isomers/conformers may be missing in a metadynamics trajectory due to chaotic nature of the trajectory. The latter case of incomplete structural sampling may manifest itself in structurally flexible systems (many conformers and low-lying isomers). Unfortunately, the complete structural sampling of flexible systems is computationally very costly. At the same time, such detailed information (all isomers/conformers) may be unnecessary for any practical purposes. *In this work,*

we aimed to show the facts of ion structural flexibility and isomerism, not to exhaustively sample all possible structures.

Alternatively, one can use the CREST code[11] for conformer/isomer sampling. CREST is provided by the developers of the `xtb` program and their collaborators. In this case, however, one may need to carefully re-tune parameters in CREST for isomer sampling. We stayed with a more straightforward approach, as it allowed us to sample isomers of ions in a black-box manner until ion fragmentation was observed in the MetaD run.

Refinement of geometries was performed using DFT methods. All Kohn-Sham DFT calculations were performed using ORCA 4.2.1. Only closed-shell ions were considered, so only spin-restricted calculations were performed. Calculations were performed using the OLYP exchange-correlation functional[12,13] with D3(BJ) dispersion corrections.[14,15] To adequately treat both cations and anions, the ma-def2-SVP basis set was used.[16] A dense integration grid was used ("GRID6"); the two-step integration procedure was switched off ("NOFINALGRID"). The second-order SCF procedure was forbidden ("NOSOSCF"). The "TightSCF" and "SlowConv" keywords were specified. We used the resolution-of-the-identity (RI) approximation[17–23] and the Def2/J auxiliary basis set for initial geometry optimizations.[24] Then, geometry optimization and normal mode analysis without the RI approximation were performed (the "NORI" option in ORCA). Notably, few NORI-optimization steps were necessary in almost all cases. All other parameters in the RI- and NORI-calculations were the same. Vibrational frequencies were calculated analytically ("ANFREQ").

Molecular electron density distributions were obtained by all-electron calculations using the ZORA method, as implemented in ORCA with the model potential (all four terms were included in the potential, "ModelPot 1, 1, 1, 1").[25,26] M06-L[27] and TPSS[28] functionals were used. The ma-ZORA-def2-TZVP basis set[16,29] from the standard ORCA library was used for all atoms except

Cu and Pd, for which "old-ZORA-TZVP" was used because of the absence of the former basis set for Pd. Again, the “TightSCF,” “SlowConv,” “NOFINALGRID,” and “NOSOSCF” options were switched on. In ZORA computations, the unpruned dense integration grid, “GRID7,” was used. The point nucleus model was used. Again, the RI approximation was used for initial geometry optimizations and the SARC/J auxiliary basis set.[24,30] Next, the final optimization was performed *without* the RI approximation. The final geometries and the corresponding electron wave functions (“NORI”) in the MOLDEN format were used in the QTAIM analysis. For that, we converted MOLDEN files into the WFX format using the Molden2AIM program (ver. 4.3.0).

We used the AIMAll program (version 19.10.12, Professional)[31] for the QTAIM analysis. Critical point connectivity was determined using the “Complex” mechanism. The automatic choice of an integration algorithm (AIMAll default) with a “Very Fine IAS mesh” and a basin quadrature of a “Very High” accuracy was selected for basin integration. Atomic source contributions were included.

Avogadro molecular editor[32] and POVRay[33] were used for the visualization of molecular geometries. Jmol was used for rendering the MD and MetaD trajectories.[34]

5. Isomer Structures and Energies Predicted with GFN2-xTB

Table S2. Structures of anions in the spectra, as predicted with GFN2-xTB. Bonds (sticks) between atoms are shown to guide the eye only. Atom-atom interactions are better represented in the QTAIM analysis given in Section 2.7.

Ion molecular formula	Low-energy isomers[a]	Fragmentation in MetaD[b]
CuCl solution in CH_3CN, negative ion mode		
$[Cu_5Cl_6]^-$	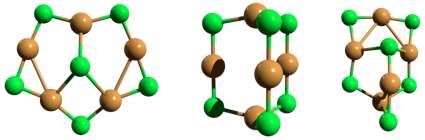 *iso1* 0.0 kcal/mol *iso2* 0.4 *iso3* 5.9	⟶ $[Cu_3Cl_3]$ + $[CuCl_2]^-$ (*) + [CuCl]
$PdCl_2$ solution in CH_3CN, negative ion mode		
$[Cu_3Pd_4Cl_{12}(O_2)]^-$	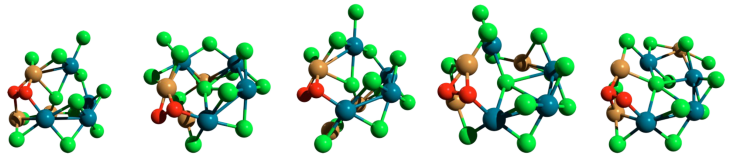 *iso1* 0.0 kcal/mol *iso2* 0.8 *iso3* 1.4 *iso4* 8.2 *iso5* 9.9	None[c]

$[Pd_5Cl_{11}]^-$	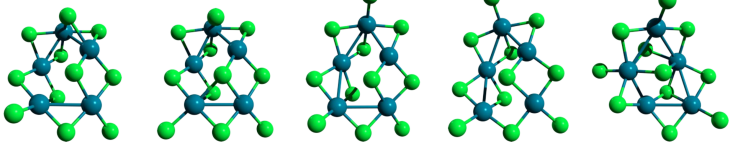 *iso1* 0.0 kcal/mol *iso2* 2.5 *iso3* 5.1 *iso4* 5.4 *iso5* 8.3	None[c]
The mixture of $PdCl_2$ and CuCl solutions in CH_3CN, negative ion mode		
$[Cu_3Pd_2Cl_8]^-$	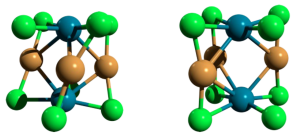 *iso1* 0.0 kcal/mol *iso2* 2.9	$\longrightarrow [Cu_2Pd_2Cl_7]^-$ (*) + [CuCl]
$[Cu_3Pd_3Cl_{10}(O_2)]^-$	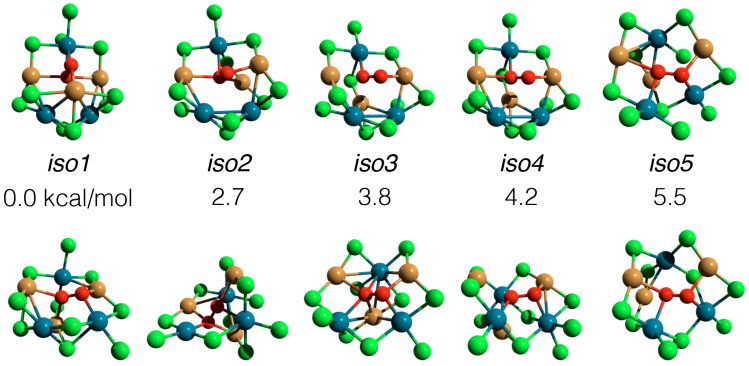 *iso1* 0.0 kcal/mol *iso2* 2.7 *iso3* 3.8 *iso4* 4.2 *iso5* 5.5 *iso6* 5.6 kcal/mol *iso7* 6.6 *iso8* 6.7 *iso9* 6.9 *iso10* 9.5	None[c]

$[Cu_3Pd_6Cl_{16}]^-$	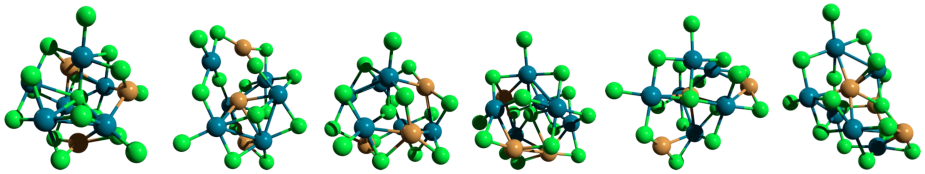 *iso1* 0.0 kcal/mol *iso2* 1.4 *iso3* 2.6 *iso4* 2.8 *iso5* 5.8 *iso6* 7.1	None[c]

[a] Relative U (in kcal/mol) is shown below each isomer if several isomers were found. [b] An asterisk in parentheses indicates that the fragmentation product was also detected in the experimental spectrum. [c] Ion took linear conformation at the end of the MetaD trajectory, as opposed to the folded conformation in the beginning.

Table S3. Structures of cations in spectra, as predicted with GFN2-xTB. Bonds (sticks) between atoms are shown to guide the eye only. Atom-atom interactions are better represented in the QTAIM analysis given in Section 2.7.

Ion molecular formula	Low-energy isomers[a]	Fragmentation in MetaD[b]
CuCl solution in CH_3CN, positive ion mode		
$[Cu(CH_3CN)(N_2)]^+$	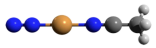 *iso1*	None
$[Cu_2Cl(CH_3CN)(H_2O)]^+$	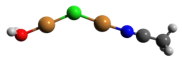 *iso1*	$\longrightarrow [Cu_2Cl(CH_3CN)]^+$ (*) + $H_2O \longrightarrow [Cu_2Cl]^+$ (*) + CH_3CN + H_2O
$[Cu_2Cl(CH_3CN)(N_2)]^+$	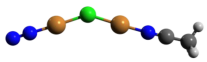 *iso1*	$\longrightarrow [CuCl\ (N_2)] + CH_3CN + Cu^+ \longrightarrow [CuCl\ (N_2)]$ + $[Cu\ (CH_3CN)]^+$ (*)
$[Cu_3Cl_2(CH_3CN)(N_2)]^+$	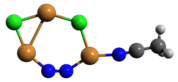 *iso1* 0.0 kcal/mol 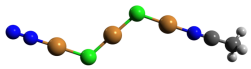 *iso2* 0.7	$\longrightarrow [Cu_2Cl_2] + [Cu(CH_3CN)(N_2)]^+$ (*)
$PdCl_2$ solution in CH_3CN, positive ion mode		
$[Pd_2Cl_3(CH_3CN)_2(H_2O)]^+$	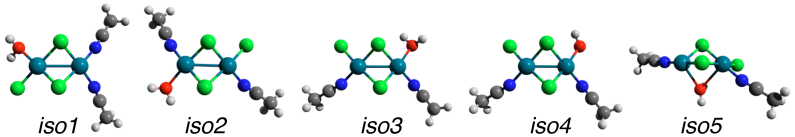 *iso1* 0.0 kcal/mol *iso2* 1.8 *iso3* 2.1 *iso4* 2.9 *iso5* 3.6	$\longrightarrow [Pd_2Cl_3(CH_3CN)(H_2O)]^+ + CH_3CN$

$[Pd_2Cl_3(CH_3CN)_2(N_2)]^+$	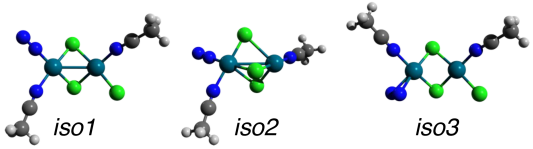 *iso1* 0.0 kcal/mol *iso2* 5.2 *iso3* 6.1	$\longrightarrow [Pd_2Cl_3(CH_3CN)(N_2)]^+ + CH_3CN$
Mixture of $PdCl_2$ and CuCl solutions in CH_3CN, positive ion mode		
$[Cu_2Pd_2Cl_5(CH_3CN)_2]^+$	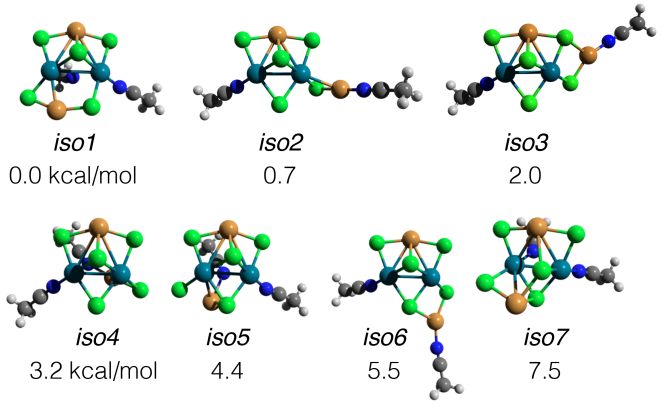 *iso1* 0.0 kcal/mol *iso2* 0.7 *iso3* 2.0 *iso4* 3.2 kcal/mol *iso5* 4.4 *iso6* 5.5 *iso7* 7.5	$\longrightarrow [Cu_2Pd_2Cl_5(CH_3CN)]^+ + CH_3CN$

[a] Relative U (in kcal/mol) is shown below each isomer if several isomers were found. [b] An asterisk in parentheses indicates that the fragmentation product was also detected in the experimental spectrum.

6. QTAIM Analysis of Ion Isomers

6.1. Ions in Spectra of CuCl

6.1.1. Monoanions

$[Cu_5Cl_6]^-$ (iso2), ZORA-M06-L/triple-ζ*

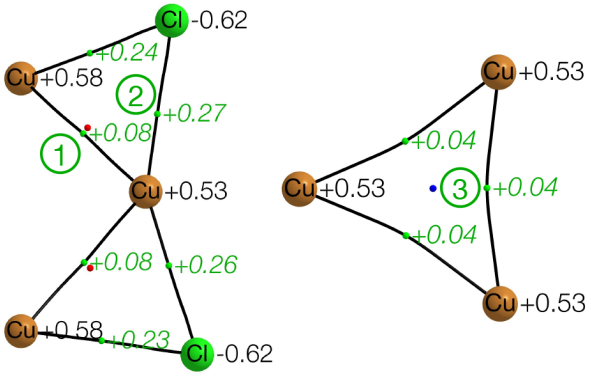

Bader charges are shown near corresponding atoms (regular black typeface). Values of $\nabla^2\rho_b$ are shown near corresponding bond critical points (*green italics*).

Bond	ρ_b**	$\nabla^2\rho_b$	$\frac{G(r_b)}{\rho_b}$	$\frac{h_e(r_b)}{\rho_b}$	$\delta(A,B)$	ε_b	$q(A)$,$q(B)$	$\oint_{A\cap B}\rho(r_b)$	Bond type
1	0.04	0.08	0.70	-0.13	0.24	2.71... 3.11***	+0.58 (Cu1), +0.53(Cu2)	0.21	Weak metal-metal
2	0.08	0.27	1.14	-0.30	0.68	0.03	+0.53 (Cu2), -0.62(Cl)	0.64	Donor-acceptor
3	0.03	0.04	0.52	-0.16	0.20	1.03	+0.53(Cu2), +0.53(Cu2')	0.15	Weak metal-metal

* Some atoms were omitted for clarity; see the main text for the whole optimized structure. The electron density distribution was obtained at the ZORA-M06L/ma-ZORA-def2-TZVP level; the "old-ZORA-TZVP" basis set from the standard ORCA 4.2.1 was used for Cu and Pd (see below) atoms.

****Disambiguation.** ρ_b is the electron density at the bond critical point (BCP), $\nabla^2\rho_b$ is the Laplacian of electron density at the BCP, ε_b is the bond ellipticity, $G(r_b)$ is the positive definite kinetic energy density at the BCP, $h_e(r_b)$ is the electron energy density at the BCP, $\delta(A,B)$ is the QTAIM bond delocalization index, q(A) and q(B) are Bader charges, and $\oint_{A\cap B}\rho(r_b)$ is the integral of electron density over the interatomic surface separating atoms A and B.

*** Varies from atom to atom.

$[Cu_5Cl_6]^-$ (iso2), ZORA-TPSS/triple-ζ*

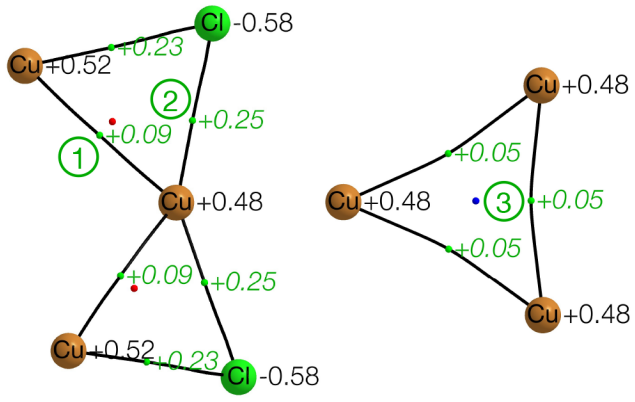

Bader charges are shown near corresponding atoms (black regular typeface). Values of $\nabla^2\rho_b$ are shown near corresponding bond critical points (*green italics*).

Bond	ρ_b	$\nabla^2\rho_b$	$\frac{G(r_b)}{\rho_b}$	$\frac{h_e(r_b)}{\rho_b}$	$\delta(A,B)$	ε_b	$q(A)$,$q(B)$	$\oint_{A\cap B}\rho(r_b)$	Bond type
1	0.04	0.09	0.71	-0.15	0.27	1.02	+0.52(Cu1), +0.48(Cu2)	0.24	Weak metal-metal
2	0.08	0.25	1.08	-0.30	0.70	0.03	+0.48(Cu2), -0.58(Cl)	0.64	Donor-acceptor
3	0.03	0.05	0.56	-0.16	0.24	0.94	+0.48(Cu2), +0.48(Cu2')	0.18	Weak metal-metal

* Some atoms were omitted for clarity; see the main text for the whole optimized structure. The electron density distribution was obtained at the ZORA-TPSS/ma-ZORA-def2-TZVP level; the "old-ZORA-TZVP" basis set from the standard ORCA 4.2.1 was used for Cu and Pd (see below) atoms.

6.1.2. Monocations

[Cu(CH$_3$CN)(N$_2$)]$^+$, ZORA-M06-L/triple-ζ

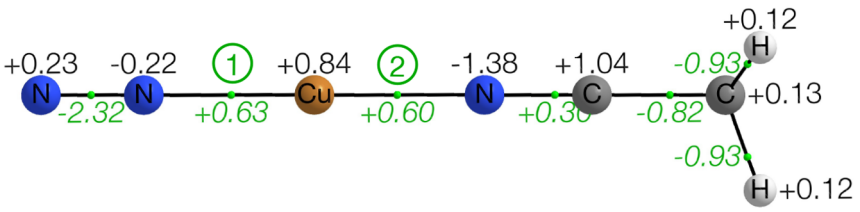

Bond	ρ_b	$\nabla^2\rho_b$	$\frac{G(r_b)}{\rho_b}$	$\frac{h_e(r_b)}{\rho_b}$	$\delta(A,B)$	ε_b	$q(A)$,$q(B)$	$\oint_{A\cap B}\rho(r_b)$	Bond type
1	0.12	0.63	1.69	-0.38	0.71	0.00	+0.84(Cu), -0.22(N)	0.69	Donor-acceptor
2	0.13	0.60	1.59	-0.39	0.72	0.00	+0.84(Cu), -1.38(N)	0.72	Donor-acceptor

[Cu(CH$_3$CN)(N$_2$)]$^+$, ZORA-TPSS/triple-ζ

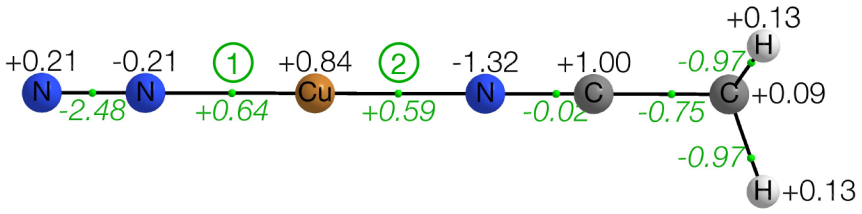

Bond	ρ_b	$\nabla^2\rho_b$	$\frac{G(r_b)}{\rho_b}$	$\frac{h_e(r_b)}{\rho_b}$	$\delta(A,B)$	ε_b	$q(A)$,$q(B)$	$\oint_{A\cap B}\rho(r_b)$	Bond type
1	0.13	0.64	1.66	-0.41	0.76	0.00	+0.84(Cu), -0.21(N)	0.73	Donor-acceptor
2	0.13	0.59	1.54	-0.41	0.75	0.00	+0.84(Cu), -1.32(N)	0.74	Donor-acceptor

$[Cu_2Cl(CH_3CN)(H_2O)]^+$, ZORA-M06-L/triple-ζ

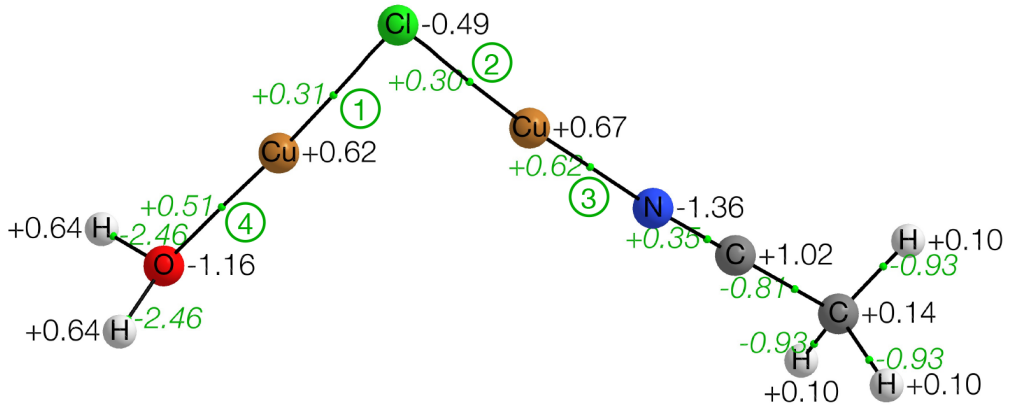

Bond	ρ_b	$\nabla^2\rho_b$	$\frac{G(r_b)}{\rho_b}$	$\frac{h_e(r_b)}{\rho_b}$	$\delta(A,B)$	ε_b	$q(A)$,$q(B)$	$\oint_{A\cap B}\rho(r_b)$	Bond type
1	0.10	0.31	1.16	-0.38	0.85	0.03	+0.62(Cu), -0.49(Cl)	0.87	Donor-acceptor
2	0.09	0.30	1.16	-0.37	0.79	0.02	-0.49(Cl), +0.67(Cu)	0.84	Donor-acceptor
3	0.12	0.62	1.64	-0.38	0.75	0.00	+0.67(Cu), -1.36(N)	0.74	Donor-acceptor
4	0.09	0.51	1.70	-0.24	0.53	0.04	+0.62(Cu), -1.16(O)	0.54	Donor-acceptor

$[Cu_2Cl(CH_3CN)(H_2O)]^+$, ZORA-TPSS/triple-ζ

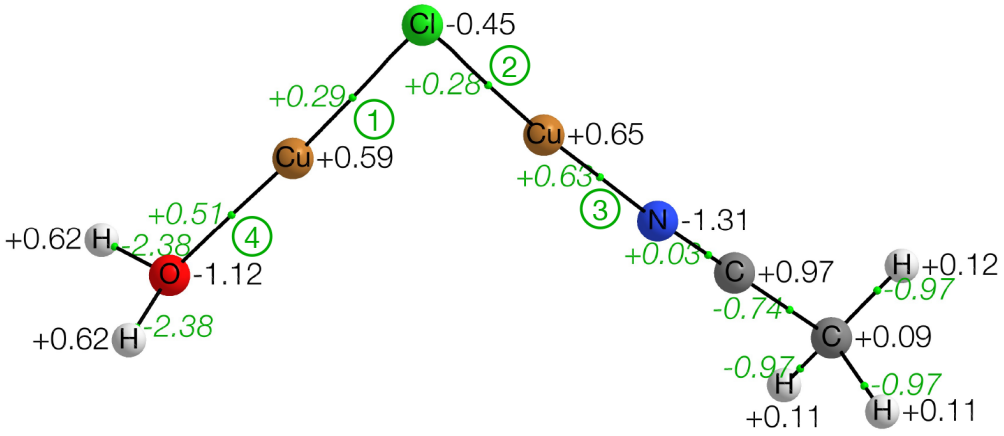

Bond	ρ_b	$\nabla^2\rho_b$	$\frac{G(r_b)}{\rho_b}$	$\frac{h_e(r_b)}{\rho_b}$	$\delta(A,B)$	ε_b	$q(A)$,$q(B)$	$\oint_{A\cap B}\rho(r_b)$	Bond type
1	0.10	0.29	1.12	-0.38	0.89	0.03	+0.59(Cu), -0.45(Cl)	0.91	Donor-acceptor
2	0.10	0.28	1.11	-0.37	0.83	0.02	-0.45(Cl), +0.65(Cu)	0.88	Donor-acceptor
3	0.13	0.63	1.61	-0.40	0.79	0.00	+0.65(Cu), -1.31(N)	0.77	Donor-acceptor
4	0.09	0.51	1.64	-0.27	0.56	0.03	+0.59(Cu), -1.12(O)	0.57	Donor-acceptor

$[Cu_2Cl(CH_3CN)(N_2)]^+$, ZORA-M06-L/triple-ζ

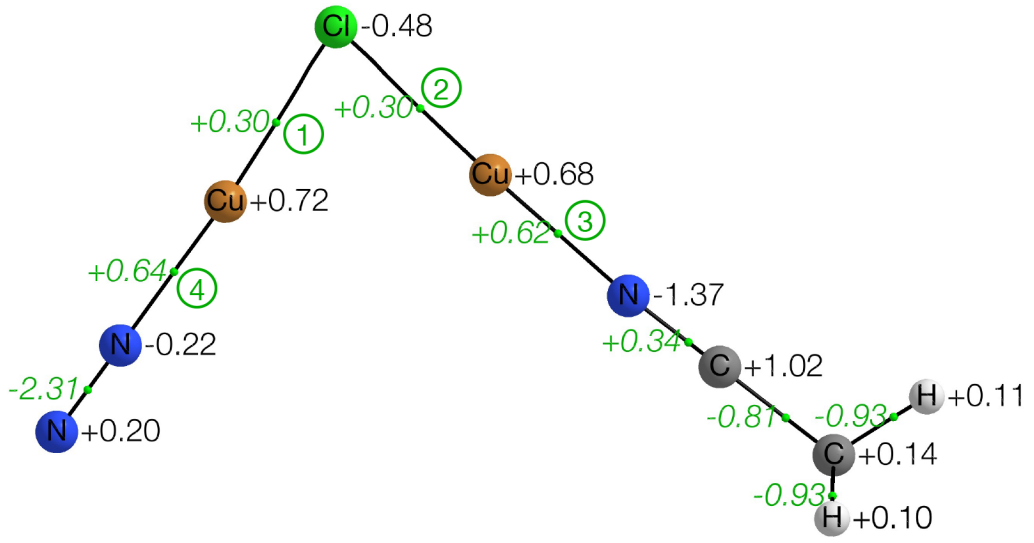

Bond	ρ_b	$\nabla^2\rho_b$	$\frac{G(r_b)}{\rho_b}$	$\frac{h_e(r_b)}{\rho_b}$	$\delta(A,B)$	ε_b	$q(A)$,$q(B)$	$\oint_{A\cap B}\rho(r_b)$	Bond type
1	0.10	0.30	1.15	-0.38	0.82	0.02	+0.72(Cu), -0.48(Cl)	0.84	Donor-acceptor
2	0.09	0.30	1.17	-0.37	0.80	0.02	-0.48(Cl), +0.68(Cu)	0.82	Donor-acceptor
3	0.12	0.62	1.63	-0.38	0.74	0.00	+0.68(Cu), -1.37(N)	0.73	Donor-acceptor
4	0.12	0.64	1.71	-0.38	0.73	0.00	+0.72(Cu), -0.22(N)	0.71	Donor-acceptor

$[Cu_2Cl(CH_3CN)(N_2)]^+$, ZORA-TPSS/triple-ζ

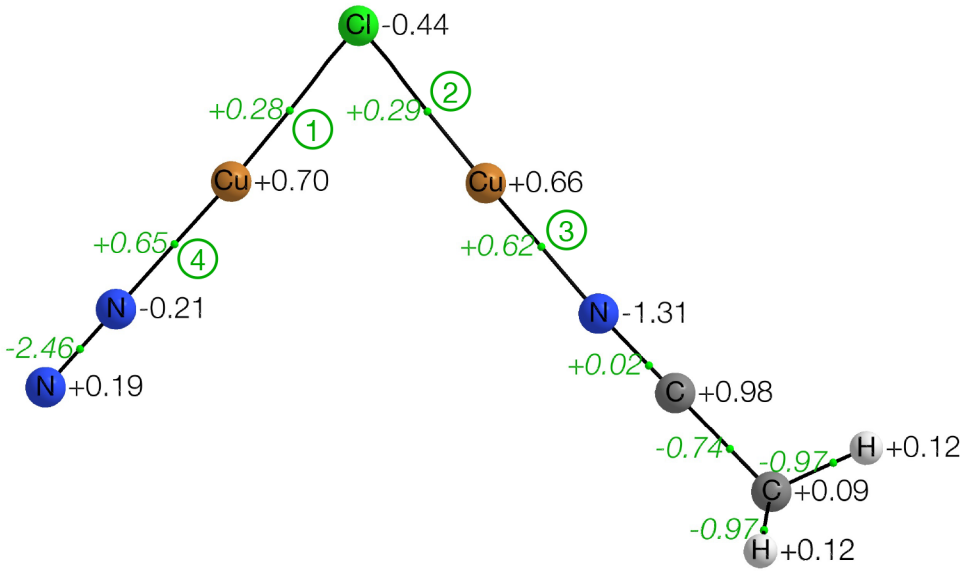

Bond	ρ_b	$\nabla^2\rho_b$	$\frac{G(r_b)}{\rho_b}$	$\frac{h_e(r_b)}{\rho_b}$	$\delta(A,B)$	ε_b	$q(A)$,$q(B)$	$\oint_{A\cap B}\rho(r_b)$	Bond type
1	0.10	0.28	1.10	-0.38	0.84	0.02	+0.70(Cu), -0.44(Cl)	0.86	Donor-acceptor
2	0.10	0.29	1.12	-0.37	0.84	0.02	-0.44(Cl), +0.66(Cu)	0.86	Donor-acceptor
3	0.13	0.62	1.60	-0.40	0.78	0.00	+0.66(Cu), -1.31(N)	0.77	Donor-acceptor
4	0.13	0.65	1.68	-0.41	0.77	0.00	+0.70(Cu), -0.21(N)	0.75	Donor-acceptor

$[Cu_3Cl_2(CH_3CN)(N_2)]^+$ (iso1), ZORA-M06-L/triple-ζ

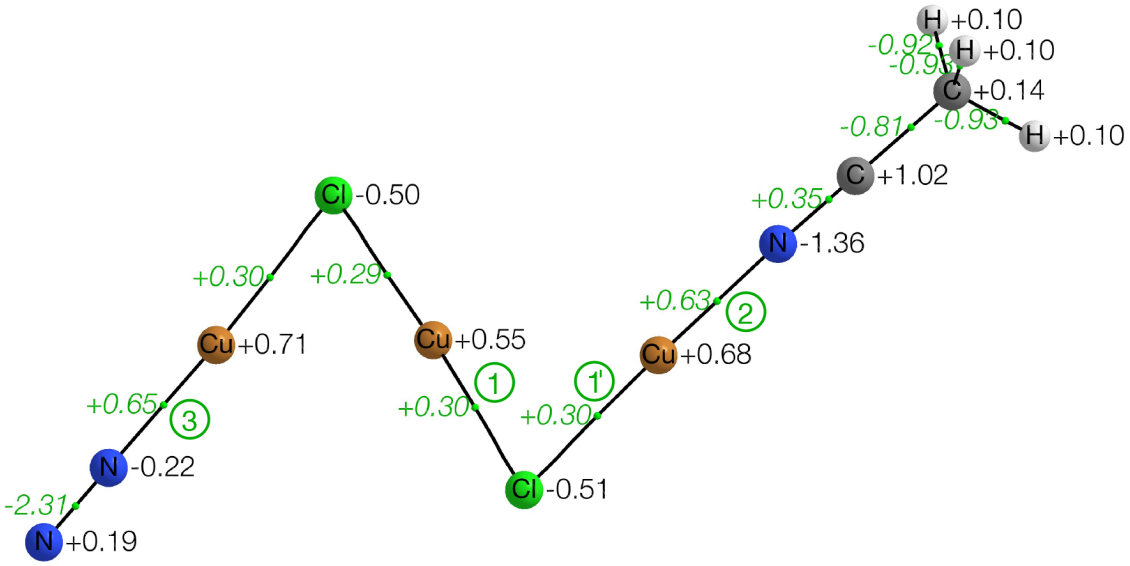

Bond	ρ_b	$\nabla^2\rho_b$	$\frac{G(r_b)}{\rho_b}$	$\frac{h_e(r_b)}{\rho_b}$	$\delta(A,B)$	ε_b	$q(A)$,$q(B)$	$\oint_{A\cap B}\rho(r_b)$	Bond type
1	0.09	0.30	1.17	-0.35	0.79	0.03	+0.55(Cu), -0.51(Cl)	0.84	Donor-acceptor
1'	0.09	0.30	1.16	-0.37	0.80	0.02	-0.51(Cl), +0.68(Cu)	0.84	Donor-acceptor
2	0.12	0.63	1.64	-0.38	0.74	0.00	+0.68(Cu), -1.36(N)	0.74	Donor-acceptor
3	0.12	0.65	1.71	-0.38	0.73	0.00	+0.71(Cu), -0.22(N)	0.71	Donor-acceptor

$[Cu_3Cl_2(CH_3CN)(N_2)]^+$ (iso1), ZORA-TPSS/triple-ζ

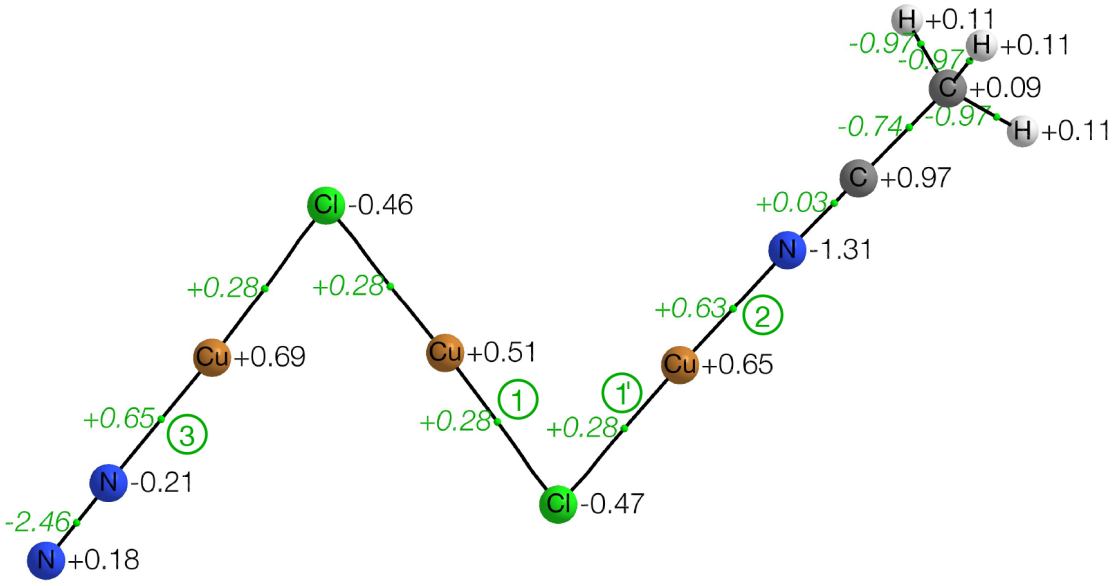

Bond	ρ_b	$\nabla^2\rho_b$	$\frac{G(r_b)}{\rho_b}$	$\frac{h_e(r_b)}{\rho_b}$	$\delta(A,B)$	ε_b	$q(A)$,$q(B)$	$\oint_{A\cap B}\rho(r_b)$	Bond type
1	0.09	0.28	1.12	-0.36	0.82	0.03	+0.51(Cu), -0.47(Cl)	0.88	Donor-acceptor
1'	0.10	0.28	1.12	-0.37	0.83	0.02	-0.47(Cl), +0.65(Cu)	0.88	Donor-acceptor
2	0.13	0.63	1.61	-0.40	0.79	0.00	+0.65(Cu), -1.31(N)	0.77	Donor-acceptor
3	0.13	0.65	1.68	-0.41	0.77	0.00	+0.69(Cu), -0.21(N)	0.75	Donor-acceptor

$[Cu_3Cl_2(CH_3CN)(N_2)]^+$ (iso2), ZORA-M06-L/triple-ζ

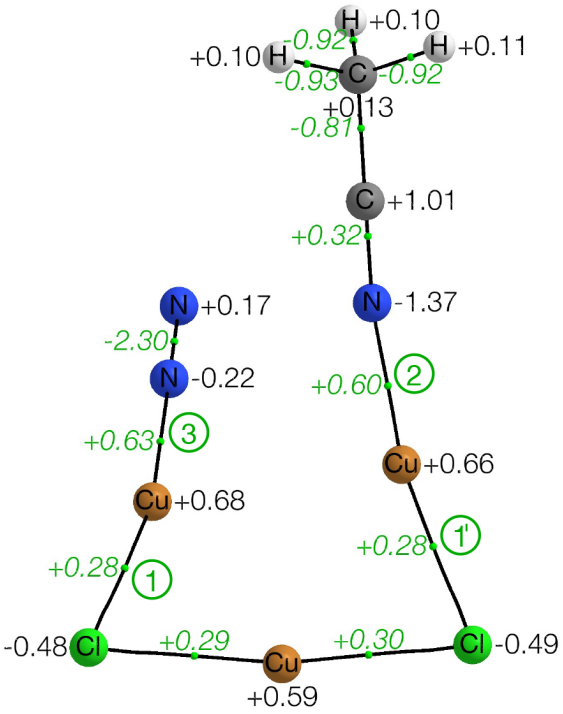

Bond	ρ_b	$\nabla^2\rho_b$	$\frac{G(r_b)}{\rho_b}$	$\frac{h_e(r_b)}{\rho_b}$	$\delta(A,B)$	ε_b	$q(A)$,$q(B)$	$\oint_{A\cap B}\rho(r_b)$	Bond type
1	0.09	0.28	1.13	-0.36	0.76	0.04	+0.68(Cu), -0.48(Cl)	1.06	Donor-acceptor
1'	0.09	0.28	1.14	-0.35	0.76	0.03	-0.49(Cl), +0.66(Cu)	1.04	Donor-acceptor
2	0.12	0.60	1.62	-0.38	0.72	0.00	+0.66(Cu), -1.37(N)	0.77	Donor-acceptor
3	0.12	0.63	1.70	-0.38	0.71	0.00	+0.68(Cu), -0.22(N)	0.74	Donor-acceptor

$[Cu_3Cl_2(CH_3CN)(N_2)]^+$ (iso2), ZORA-TPSS/triple-ζ

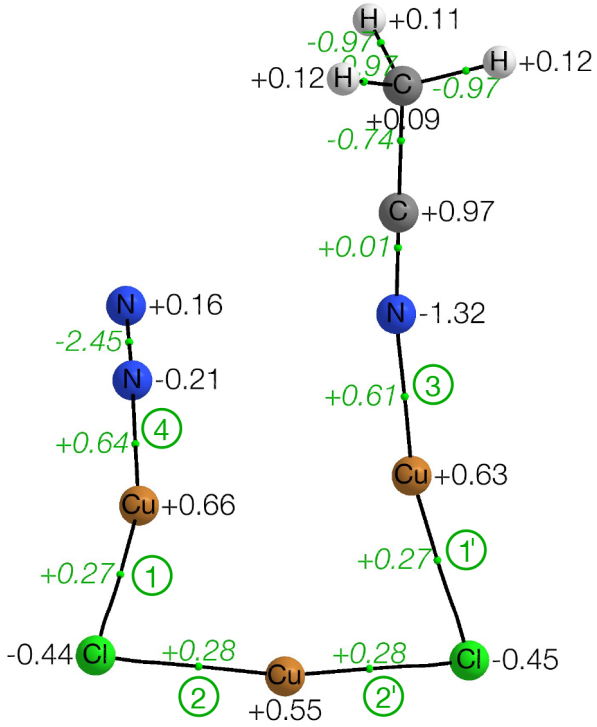

Bond	ρ_b	$\nabla^2\rho_b$	$\frac{G(r_b)}{\rho_b}$	$\frac{h_e(r_b)}{\rho_b}$	$\delta(A,B)$	ε_b	$q(A)$,$q(B)$	$\oint_{A\cap B}\rho(r_b)$	Bond type
1	0.09	0.27	1.08	-0.36	0.78	0.05	+0.66(Cu), -0.44(Cl)	1.08	Donor-acceptor
1'	0.09	0.27	1.09	-0.36	0.79	0.03	-0.45(Cl), +0.63(Cu)	1.07	Donor-acceptor
2	0.09	0.28	1.11	-0.36	0.81	0.04	-0.44(Cl), +0.55(Cu)	1.10	Donor-acceptor
2'	0.09	0.28	1.11	-0.36	0.83	0.03	+0.55(Cu), -0.45(Cl)	1.09	Donor-acceptor
3	0.13	0.61	1.59	-0.40	0.77	0.00	+0.63(Cu), -1.32(N)	0.79	Donor-acceptor
4	0.13	0.64	1.67	-0.40	0.76	0.00	+0.66(Cu), -0.21(N)	0.77	Donor-acceptor

6.2. Ions in Spectra of the Mixture of $PdCl_2$ and CuCl Solutions

6.2.1. Monoanions

$[Cu_3Pd_2Cl_8]^-$ (iso2), ZORA-M06-L/triple-ζ*

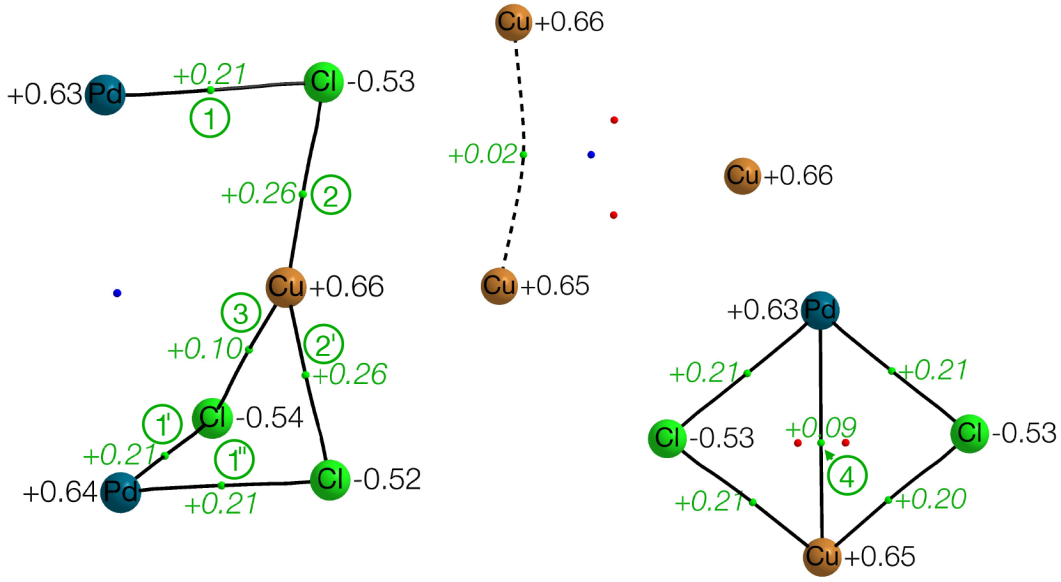

Bond	ρ_b	$\nabla^2\rho_b$	$\frac{G(r_b)}{\rho_b}$	$\frac{h_e(r_b)}{\rho_b}$	$\delta(A,B)$	ε_b	$q(A)$,$q(B)$	$\oint_{A\cap B}\rho(r_b)$	Bond type
1	0.07	0.21	0.98	-0.20	0.65	0.04	+0.63(Pd), -0.53(Cl)	0.97	Donor-acceptor
1'	0.07	0.21	0.95	-0.23	0.72	0.06	+0.64(Pd), -0.54(Cl)	0.64	Donor-acceptor
1''	0.07	0.21	0.97	-0.20	0.66	0.05	+0.64(Pd), -0.52(Cl)	0.84	Donor-acceptor
2	0.08	0.26	1.15	-0.29	0.63	0.01	-0.53(Cl), +0.66(Cu)	0.91	Donor-acceptor
2'	0.08	0.26	1.14	-0.28	0.62	0.02	+0.66(Cu), -0.52(Cl)	0.79	Donor-acceptor
3	0.03	0.10	0.85	-0.03	0.25	0.25	+0.66(Cu), -0.54(Cl)	0.25	Weak donor-acceptor
4	0.03	0.09	0.77	-0.10	0.26	0.27	+0.63(Pd), +0.65(Cu)	0.19	Weak metal-metal

* Some atoms were omitted for clarity; see the main text for the whole optimized structure.

$[Cu_3Pd_2Cl_8]^-$ (iso2), ZORA-TPSS/triple-ζ*

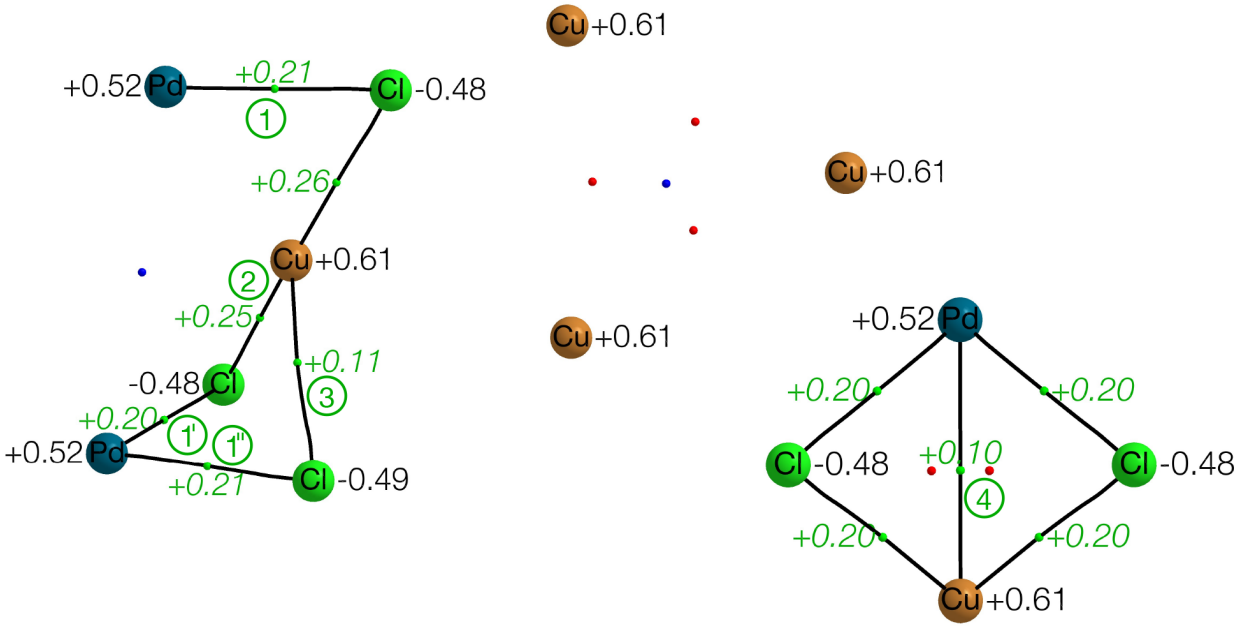

Bond	ρ_b	$\nabla^2\rho_b$	$\frac{G(r_b)}{\rho_b}$	$\frac{h_e(r_b)}{\rho_b}$	$\delta(A,B)$	ε_b	$q(A)$,$q(B)$	$\oint_{A\cap B}\rho(r_b)$	Bond type
1	0.07	0.21	0.94	-0.23	0.69	0.03	+0.52(Pd), -0.48(Cl)	1.00	Donor-acceptor
1'	0.07	0.20	0.92	-0.23	0.70	0.04	+0.52(Pd), -0.48(Cl)	0.89	Donor-acceptor
1''	0.08	0.21	0.91	-0.25	0.77	0.05	+0.52(Pd), -0.49(Cl)	0.68	Donor-acceptor
2	0.08	0.25	1.09	-0.30	0.66	0.03	-0.48(Cl), +0.61(Cu)	0.83	Donor-acceptor
3	0.04	0.11	0.86	-0.08	0.32	0.20	-0.49(Cl), +0.61(Cu)	0.31	Weak donor-acceptor
4	0.04	0.10	0.78	-0.13	0.28	0.29	+0.52(Pd), +0.61(Cu)	0.21	Weak metal-metal

* Some atoms were omitted for clarity; see the main text for the whole optimized structure.

$[Cu_3Pd_3Cl_{10}(O_2)]^-$ (iso2), ZORA-M06-L/triple-ζ

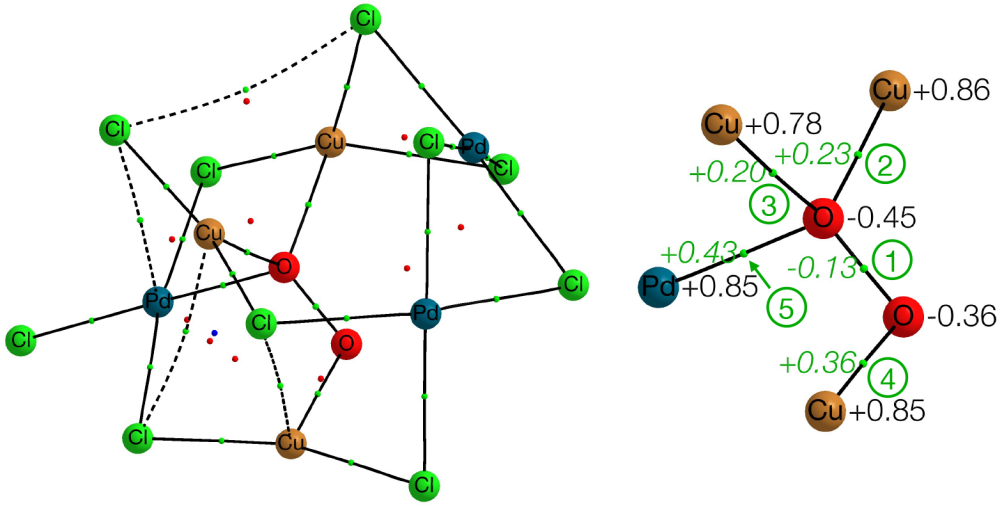

Bond	ρ_b	$\nabla^2\rho_b$	$\frac{G(r_b)}{\rho_b}$	$\frac{h_e(r_b)}{\rho_b}$	$\delta(A,B)$	ε_b	$q(A)$,$q(B)$	$\oint_{A\cap B}\rho(r_b)$	Bond type
1	0.37	-0.13	0.84	-0.92	1.37	0.00	-0.45(O1), -0.36(O2)	1.43	Covalent
2	0.05	0.23	1.16	-0.12	0.33	0.07	-0.45(O1), +0.86(Cu)	0.52	Donor-acceptor
3	0.05	0.20	1.15	-0.09	0.31	0.07	-0.45(O1), +0.78(Cu)	0.44	Donor-acceptor
4	0.09	0.36	1.31	-0.26	0.48	0.10	-0.36(O2), +0.85(Pd)	0.67	Donor-acceptor
5	0.09	0.43	1.38	-0.21	0.58	0.12	-0.45(O1), +0.85(Cu)	0.64	Donor-acceptor

$[Cu_3Pd_3Cl_{10}(O_2)]^-$ (iso2), ZORA-TPSS/triple-ζ

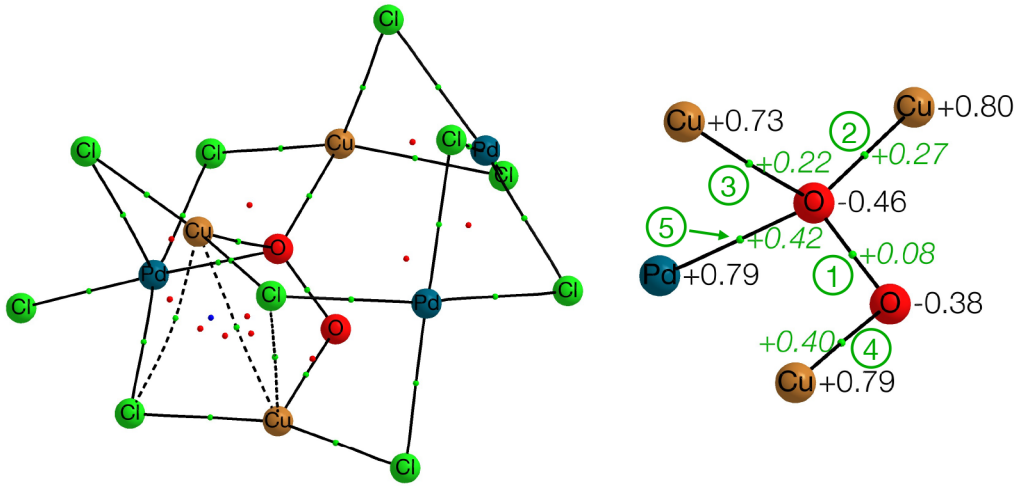

Bond	ρ_b	$\nabla^2\rho_b$	$\frac{G(r_b)}{\rho_b}$	$\frac{h_e(r_b)}{\rho_b}$	$\delta(A,B)$	ε_b	$q(A)$,$q(B)$	$\oint_{A\cap B}\rho(r_b)$	Bond type
1	0.33	0.08	0.83	-0.77	1.31	0.01	-0.46(O1), -0.38(O2)	1.34	Covalent/intermediate
2	0.07	0.27	1.20	-0.19	0.38	0.05	-0.46(O1), +0.80(Cu)	0.55	Donor-acceptor
3	0.05	0.22	1.15	-0.14	0.33	0.07	-0.46(O1), +0.73(Cu)	0.42	Donor-acceptor
4	0.10	0.40	1.33	-0.29	0.51	0.08	-0.38(O2), +0.79(Cu)	0.73	Donor-acceptor
5	0.10	0.42	1.32	-0.23	0.63	0.10	-0.46(O1), +0.79(Pd)	0.67	Donor-acceptor

$[Cu_3Pd_3Cl_{10}(O_2)]^-$ (iso4), ZORA-M06-L/triple-ζ

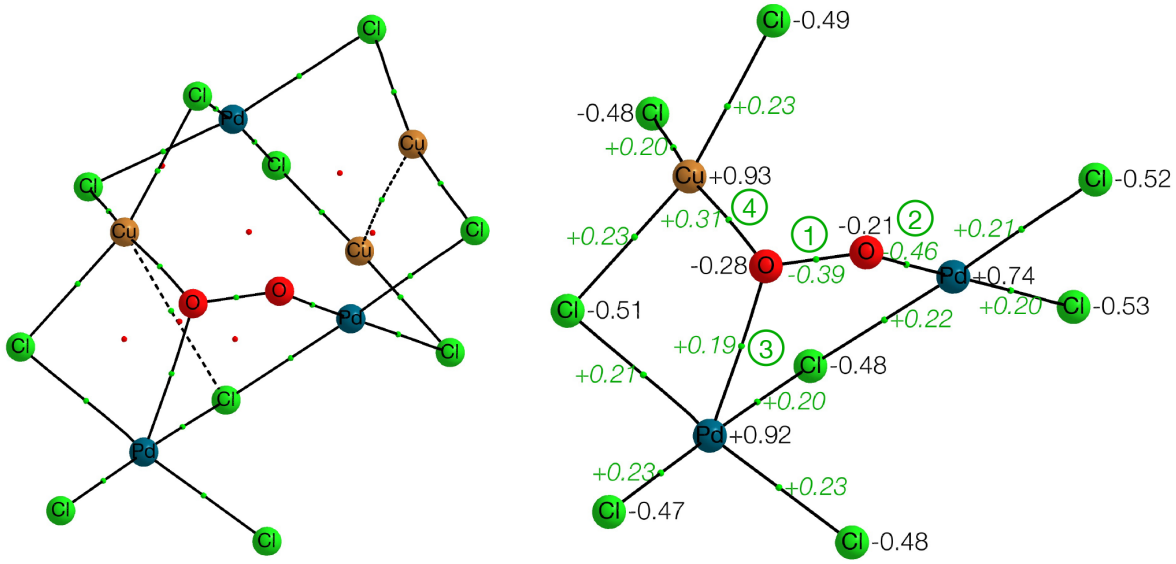

Bond	ρ_b	$\nabla^2\rho_b$	$\frac{G(r_b)}{\rho_b}$	$\frac{h_e(r_b)}{\rho_b}$	$\delta(A,B)$	ε_b	$q(A)$,$q(B)$	$\oint_{A\cap B}\rho(r_b)$	Bond type
1	0.44	-0.39	0.87	-1.10	1.49	0.01	-0.28(O1), -0.21(O2)	1.53	Covalent
2	0.11	0.46	1.29	-0.27	0.76	0.07	-0.21(O2), +0.74(Pd)	0.72	Donor-acceptor
3	0.05	0.19	1.02	-0.06	0.36	0.11	-0.28(O1), +0.92(Pd)	0.40	Weak donor-acceptor
4	0.07	0.31	1.26	-0.21	0.46	0.10	-0.28(O1), +0.93(Cu)	0.54	Weak donor-acceptor

$[Cu_3Pd_3Cl_{10}(O_2)]^-$ (iso4), ZORA-TPSS/triple-ζ

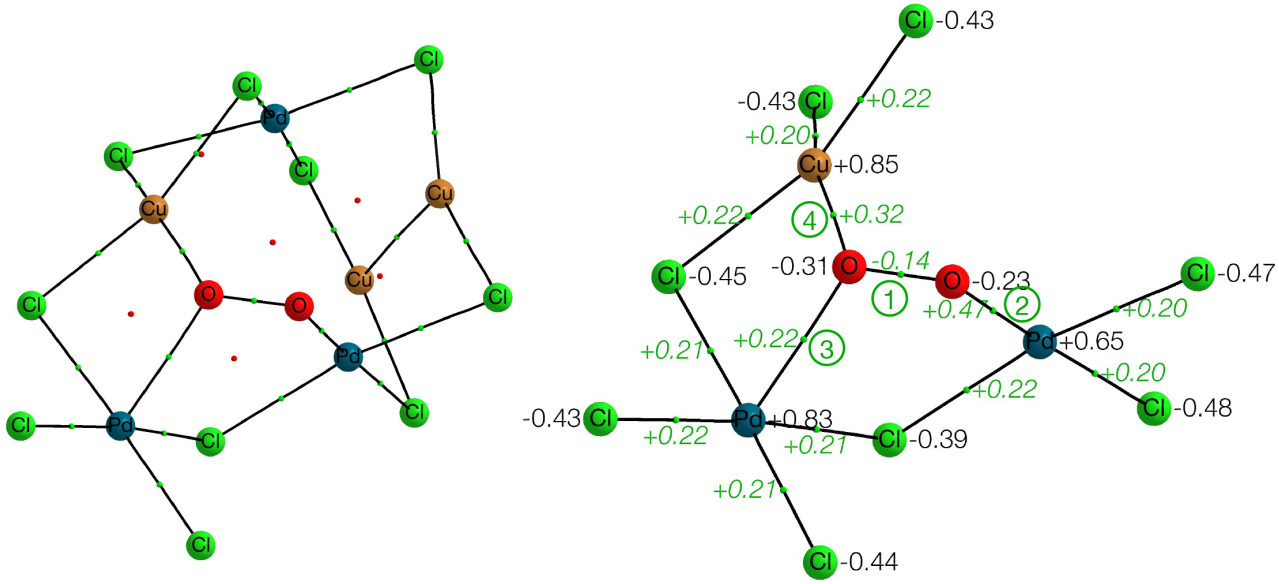

Bond	ρ_b	$\nabla^2\rho_b$	$\frac{G(r_b)}{\rho_b}$	$\frac{h_e(r_b)}{\rho_b}$	$\delta(A,B)$	ε_b	$q(A)$,$q(B)$	$\oint_{A\cap B}\rho(r_b)$	Bond type
1	0.39	-0.14	0.86	-0.95	1.44	0.02	-0.31(O1), -0.23(O2)	1.45	Covalent
2	0.12	0.47	1.28	-0.29	0.79	0.06	-0.23(O2), +0.65(Pd)	0.80	Donor-acceptor
3	0.06	0.22	1.02	-0.10	0.42	0.11	-0.31(O1), +0.83(Pd)	0.48	Weak donor-acceptor
4	0.08	0.32	1.25	-0.24	0.49	0.08	-0.31(O1), +0.85(Cu)	0.61	Weak donor-acceptor

$[Cu_3Pd_6Cl_{16}]^-$ (iso1), ZORA-M06-L/triple-ζ

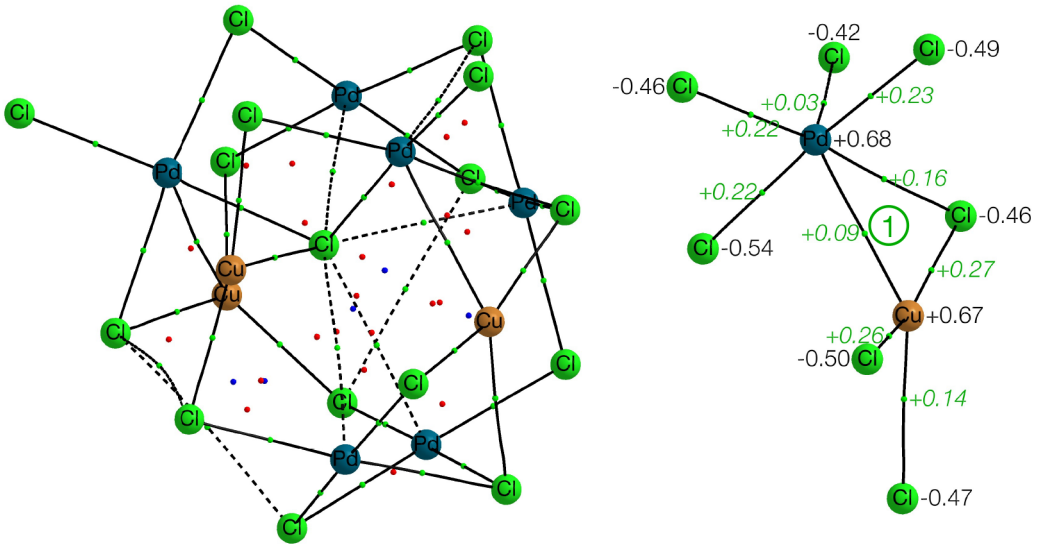

Bond	ρ_b	$\nabla^2\rho_b$	$\frac{G(r_b)}{\rho_b}$	$\frac{h_e(r_b)}{\rho_b}$	$\delta(A,B)$	ε_b	$q(A)$,$q(B)$	$\oint_{A\cap B}\rho(r_b)$	Bond type
1	0.03	0.09	0.74	-0.10	0.27	0.23	+0.67(Cu), +0.68(Pd)	0.33	Weak metal-metal

$[Cu_3Pd_6Cl_{16}]^-$ (iso1), ZORA-TPSS/triple-ζ

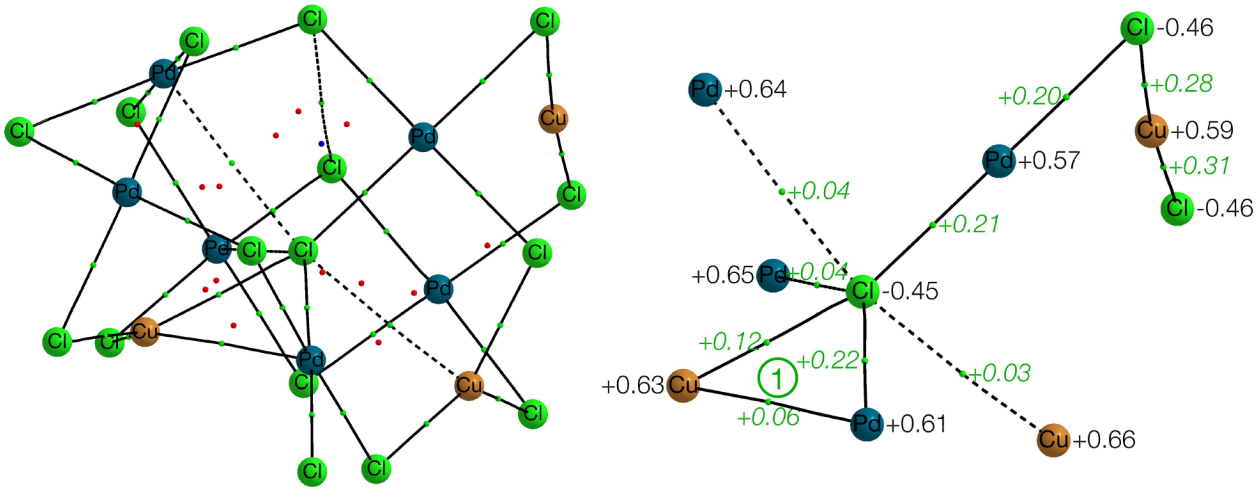

Bond	ρ_b	$\nabla^2\rho_b$	$\frac{G(r_b)}{\rho_b}$	$\frac{h_e(r_b)}{\rho_b}$	$\delta(A,B)$	ε_b	$q(A)$,$q(B)$	$\oint_{A\cap B}\rho(r_b)$	Bond type
1	0.03	0.06	0.63	-0.13	0.24	0.31	+0.63(Cu), +0.61(Pd)	0.25	Weak metal-metal

6.2.2. Monocations

$[Cu_2Pd_2Cl_5(CH_3CN)_2]^+$ (iso1), ZORA-M06-L/triple-ζ*

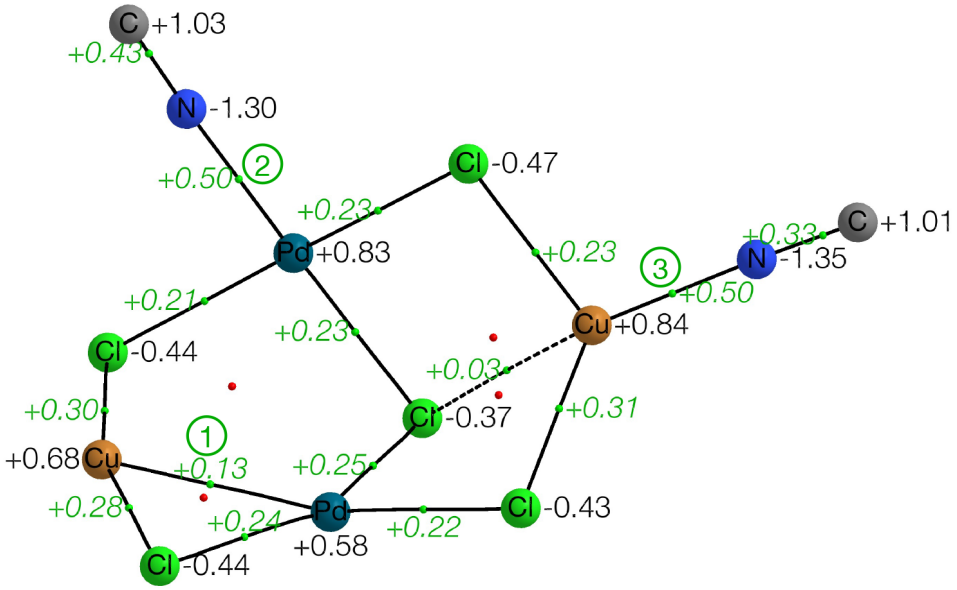

Bond	ρ_b	$\nabla^2\rho_b$	$\frac{G(r_b)}{\rho_b}$	$\frac{h_e(r_b)}{\rho_b}$	$\delta(A,B)$	ε_b	$q(A)$,$q(B)$	$\oint_{A\cap B}\rho(r_b)$	Bond type
1	0.04	0.13	0.85	-0.12	0.42	0.48	+0.68(Cu), +0.58(Pd)	0.30	Weak metal-metal
2	0.10	0.50	1.46	-0.24	0.65	0.13	+0.83(Pd), -1.30(N)	0.76	Donor-acceptor
3	0.10	0.50	1.56	-0.33	0.60	0.03	+0.84(Cu), -1.35(N)	0.65	Donor-acceptor

* CH_3 groups were omitted for clarity; see the main text for the whole optimized structure.

$[Cu_2Pd_2Cl_5(CH_3CN)_2]^+$ (iso1), ZORA-TPSS/triple-ζ*

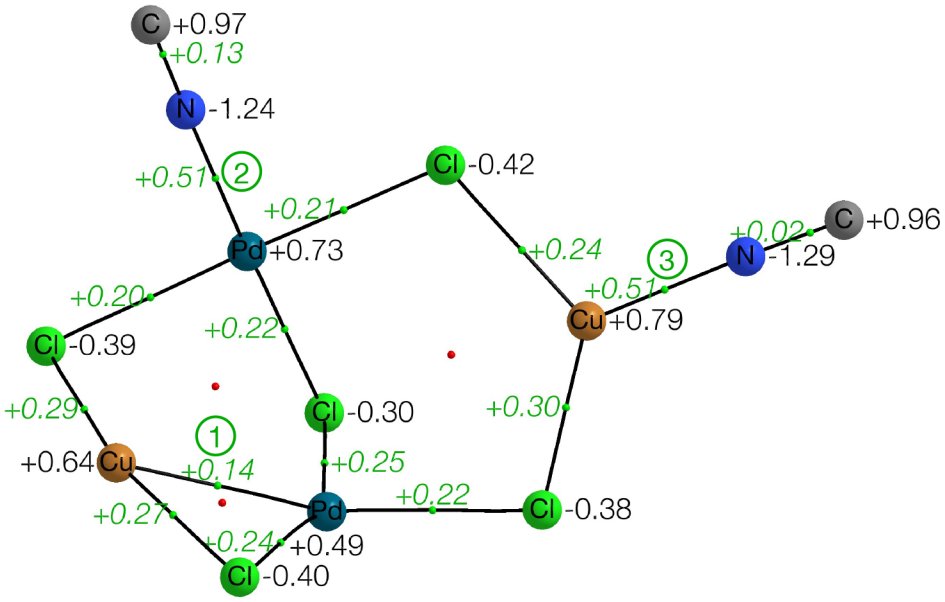

Bond	ρ_b	$\nabla^2\rho_b$	$\frac{G(r_b)}{\rho_b}$	$\frac{h_e(r_b)}{\rho_b}$	$\delta(A,B)$	ε_b	$q(A)$,$q(B)$	$\oint_{A\cap B}\rho(r_b)$	Bond type
1	0.05	0.14	0.85	-0.16	0.46	0.37	+0.64(Cu), +0.49(Pd)	0.34	Weak metal-metal
2	0.11	0.51	1.43	-0.28	0.71	0.11	+0.73(Pd), -1.24(N)	0.82	Donor-acceptor
3	0.11	0.51	1.53	-0.35	0.66	0.03	+0.79(Cu), -1.29(N)	0.70	Donor-acceptor

* CH_3 groups were omitted for clarity; see the main text for the whole optimized structure.

$[Cu_2Pd_2Cl_5(CH_3CN)_2]^+$ (iso2), ZORA-M06-L/triple-ζ*

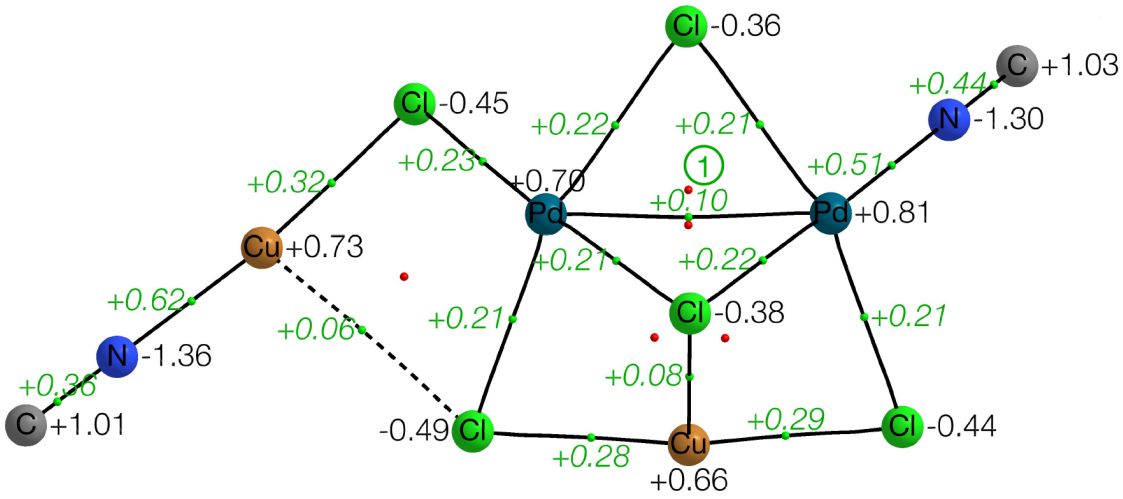

Bond	ρ_b	$\nabla^2\rho_b$	$\frac{G(r_b)}{\rho_b}$	$\frac{h_e(r_b)}{\rho_b}$	$\delta(A,B)$	ε_b	$q(A)$,$q(B)$	$\oint_{A\cap B}\rho(r_b)$	Bond type
1	0.03	0.10	0.84	-0.04	0.20	1.03	+0.70(Pd1), +0.81(Pd2)	0.11	Weak metal-metal

* CH_3 groups were omitted for clarity; see the main text for the whole optimized structure.

$[Cu_2Pd_2Cl_5(CH_3CN)_2]^+$ (iso2), ZORA-TPSS/triple-ζ*

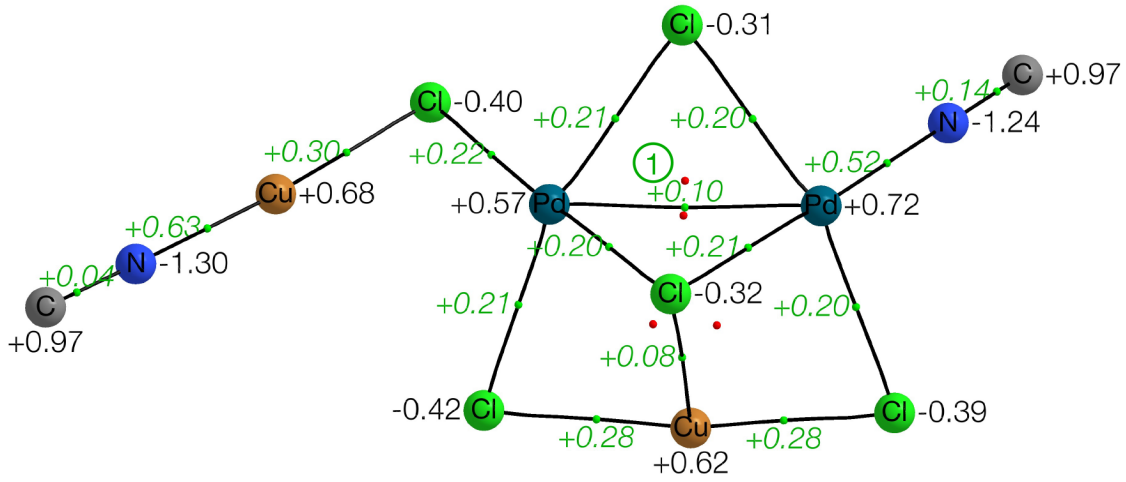

Bond	ρ_b	$\nabla^2\rho_b$	$\frac{G(r_b)}{\rho_b}$	$\frac{h_e(r_b)}{\rho_b}$	$\delta(A,B)$	ε_b	$q(A)$,$q(B)$	$\oint_{A\cap B}\rho(r_b)$	Bond type
1	0.03	0.10	0.83	-0.08	0.23	0.95	+0.57(Pd1), +0.72(Pd2)	0.12	Weak metal-metal

* CH_3 groups were omitted for clarity; see the main text for the whole optimized structure.

$[Cu_2Pd_2Cl_5(CH_3CN)_2]^+$ (iso4), ZORA-M06-L/triple-ζ

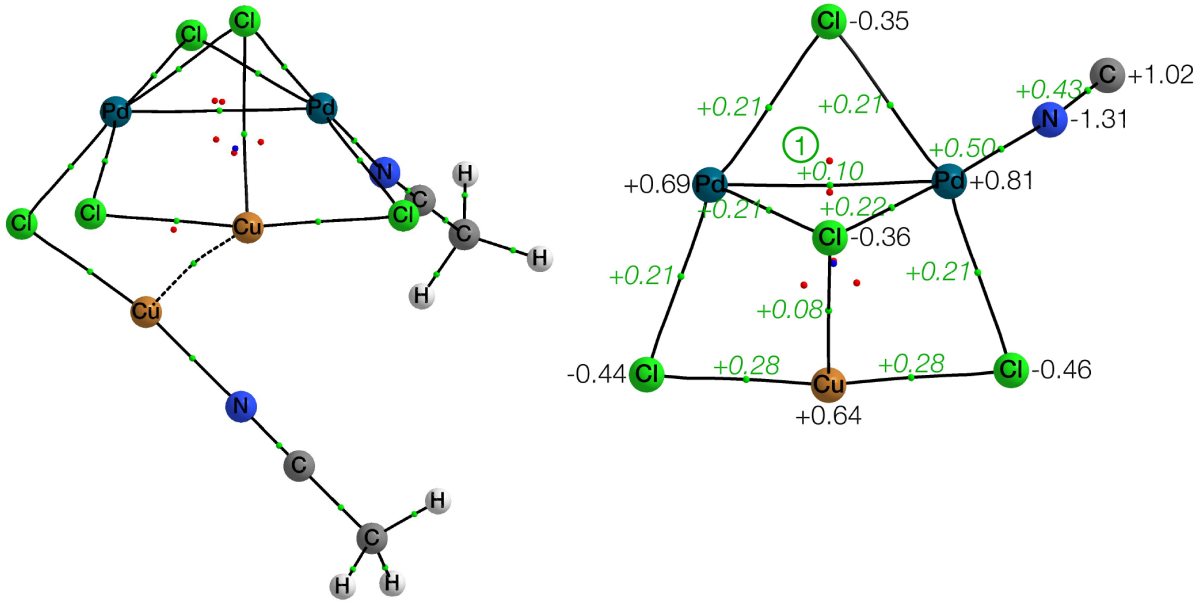

Bond	ρ_b	$\nabla^2\rho_b$	$\frac{G(r_b)}{\rho_b}$	$\frac{h_e(r_b)}{\rho_b}$	$\delta(A,B)$	ε_b	$q(A)$,$q(B)$	$\oint_{A\cap B}\rho(r_b)$	Bond type
1	0.03	0.10	0.85	-0.05	0.20	0.39	+0.69(Pd1), +0.81(Pd2)	0.16	Weak metal-metal

$[Cu_2Pd_2Cl_5(CH_3CN)_2]^+$ (iso4), ZORA-TPSS/triple-ζ

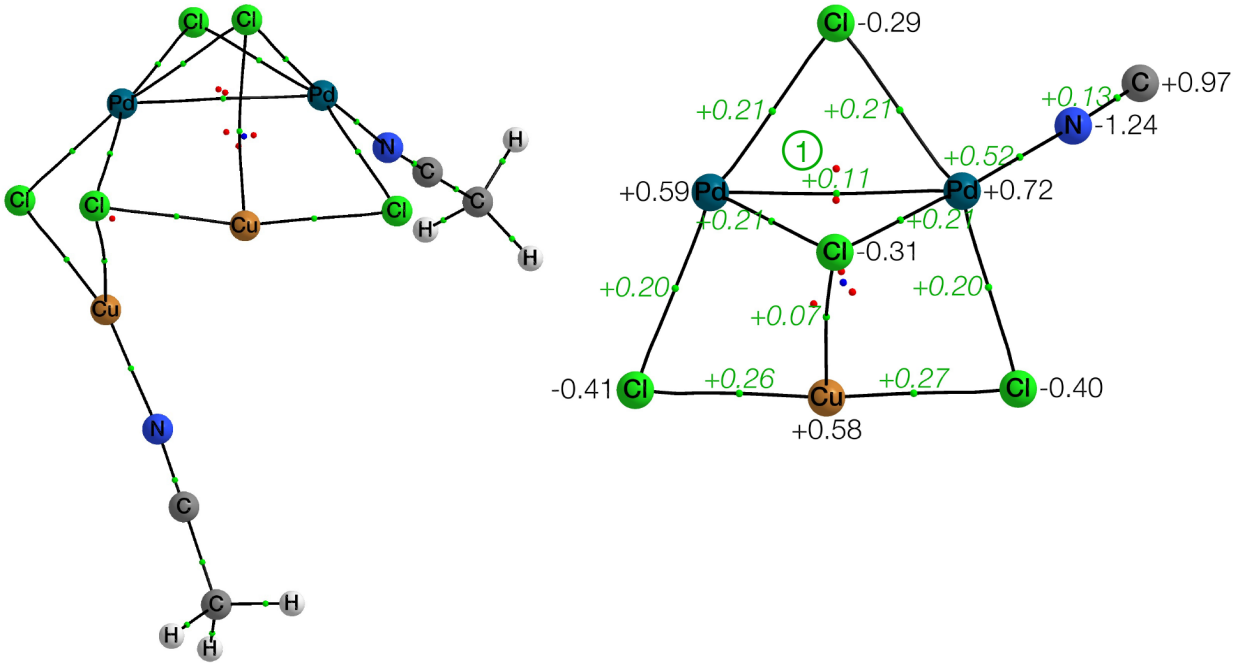

Bond	ρ_b	$\nabla^2\rho_b$	$\frac{G(r_b)}{\rho_b}$	$\frac{h_e(r_b)}{\rho_b}$	$\delta(A,B)$	ε_b	$q(A)$,$q(B)$	$\oint_{A\cap B}\rho(r_b)$	Bond type
1	0.03	0.11	0.83	-0.07	0.22	0.72	+0.59(Pd1), +0.72(Pd2)	0.13	Weak metal-metal

6.3. Ions in Spectra of $PdCl_2$

6.3.1. Monoanions

$[Cu_3Pd_4Cl_{12}(O_2)]^-$ (iso1), ZORA-M06-L/triple-ζ

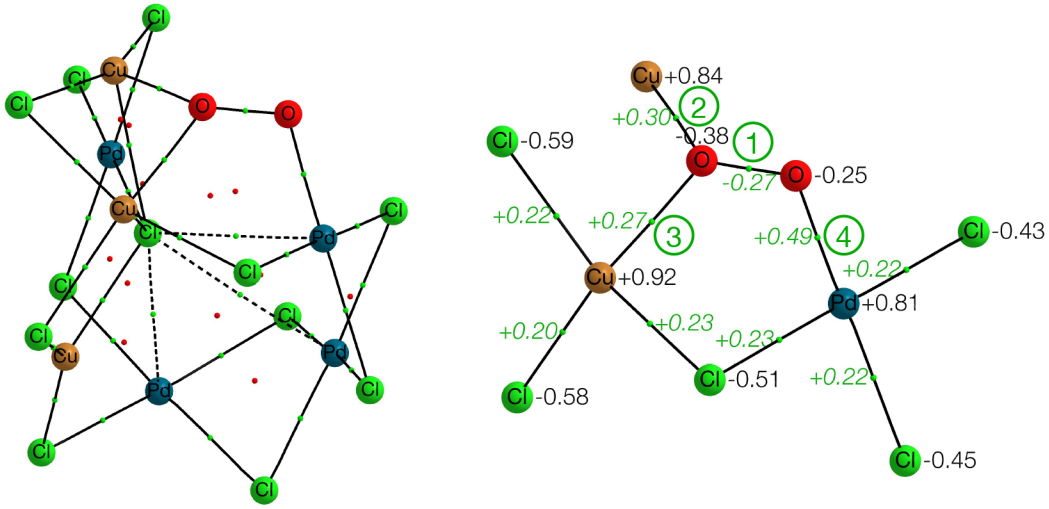

Bond	ρ_b	$\nabla^2\rho_b$	$\frac{G(r_b)}{\rho_b}$	$\frac{h_e(r_b)}{\rho_b}$	$\delta(A,B)$	ε_b	$q(A)$,$q(B)$	$\oint_{A\cap B}\rho(r_b)$	Bond type
1	0.41	-0.27	0.85	-1.02	1.42	0.02	-0.38(O1), -0.25(O2)	1.41	Covalent
2	0.07	0.30	1.28	-0.19	0.41	0.09	-0.38(O1), +0.84(Cu)	0.52	Weak donor-acceptor
3	0.06	0.27	1.25	-0.17	0.41	0.10	-0.38(O1), +0.84(Cu)	0.44	Weak donor-acceptor
4	0.12	0.49	1.31	-0.28	0.77	0.09	-0.25(O2), +0.81(Pd)	0.73	Donor-acceptor

$[Cu_3Pd_4Cl_{12}(O_2)]^-$ (iso1), ZORA-TPSS/triple-ζ

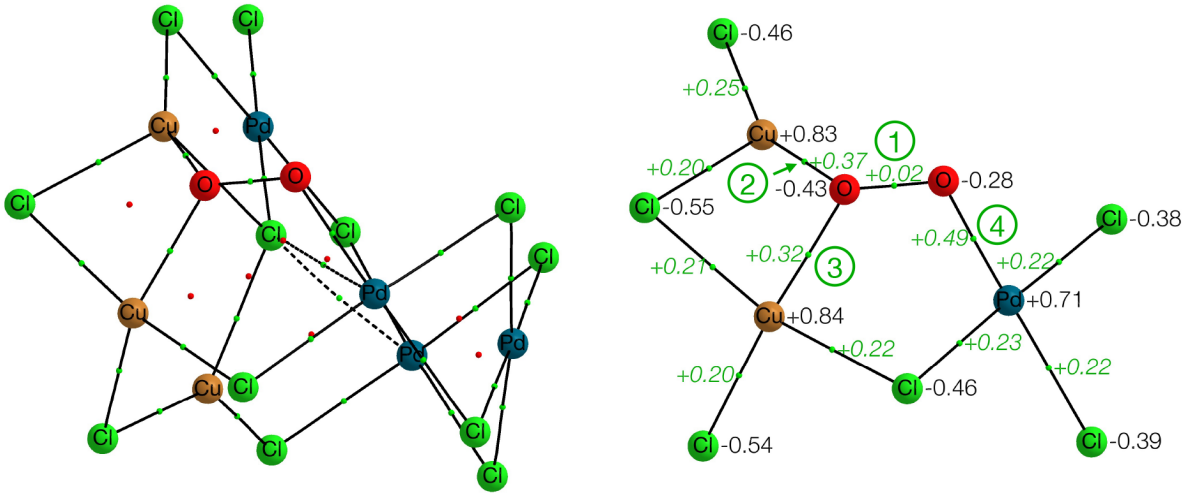

Bond	ρ_b	$\nabla^2\rho_b$	$\frac{G(r_b)}{\rho_b}$	$\frac{h_e(r_b)}{\rho_b}$	$\delta(A,B)$	ε_b	$q(A)$,$q(B)$	$\oint_{A\cap B}\rho(r_b)$	Bond type
1	0.35	0.02	0.84	-0.83	1.34	0.02	-0.43(O1), -0.28(O2)	1.28	Covalent/intermediate
2	0.09	0.37	1.32	-0.27	0.50	0.07	-0.43(O1), +0.83(Cu)	0.65	Weak donor-acceptor
3	0.07	0.32	1.31	-0.22	0.44	0.07	-0.43(O1), +0.84(Cu)	0.55	Weak donor-acceptor
4	0.12	0.49	1.30	-0.30	0.81	0.07	-0.28(O2), +0.71(Pd)	0.78	Donor-acceptor

$[Pd_5Cl_{11}]^-$ (iso1), ZORA-M06-L/triple-ζ

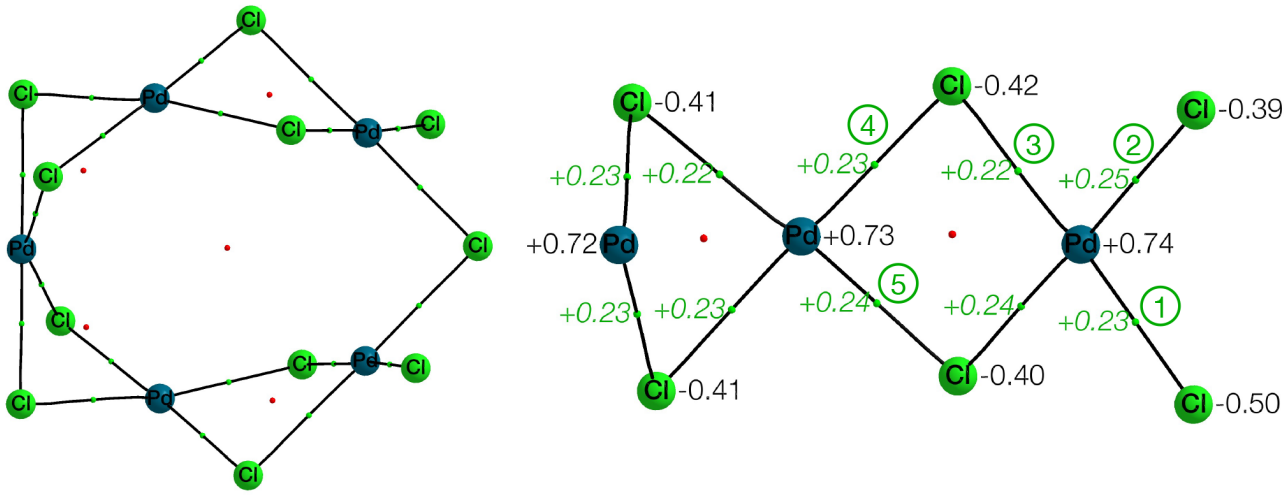

Bond	ρ_b	$\nabla^2\rho_b$	$\frac{G(r_b)}{\rho_b}$	$\frac{h_e(r_b)}{\rho_b}$	$\delta(A,B)$	ε_b	$q(A)$,$q(B)$	$\oint_{A\cap B}\rho(r_b)$	Bond type
1	0.09	0.23	0.93	-0.29	0.91	0.04	+0.74(Pd), -0.50(Cl)	0.82	Strong donor-acceptor
2	0.08	0.25	1.03	-0.24	0.73	0.09	+0.74(Pd), -0.39(Cl)	0.88	Donor-acceptor
3	0.06	0.22	1.05	-0.17	0.58	0.04	+0.74(Pd), -0.42(Cl)	0.64	Donor-acceptor
4	0.08	0.23	0.98	-0.25	0.77	0.07	+0.73(Pd), -0.42(Cl)	0.68	Donor-acceptor
5	0.08	0.24	0.99	-0.25	0.76	0.07	+0.73(Pd), -0.40(Cl)	0.69	Donor-acceptor

$[Pd_5Cl_{11}]^-$ (iso1), ZORA-TPSS/triple-ζ

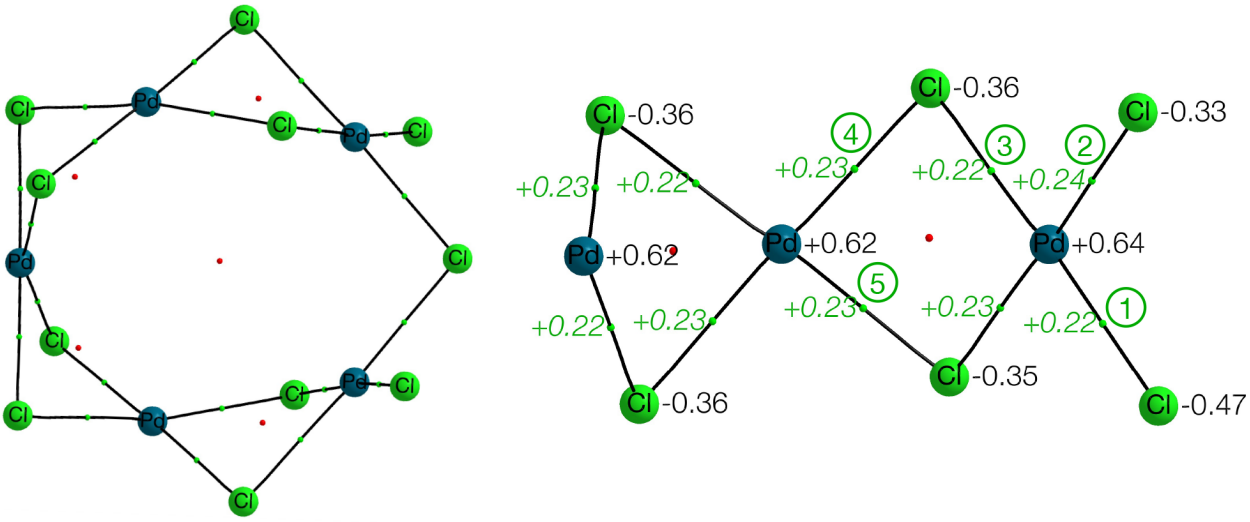

Bond	ρ_b	$\nabla^2\rho_b$	$\frac{G(r_b)}{\rho_b}$	$\frac{h_e(r_b)}{\rho_b}$	$\delta(A,B)$	ε_b	$q(A)$,$q(B)$	$\oint_{A\cap B}\rho(r_b)$	Bond type
1	0.09	0.22	0.89	-0.30	0.94	0.04	+0.64(Pd), -0.47(Cl)	0.85	Strong donor-acceptor
2	0.08	0.24	0.99	-0.27	0.78	0.08	+0.64(Pd), -0.33(Cl)	0.85	Donor-acceptor
3	0.07	0.22	1.00	-0.22	0.65	0.03	+0.64(Pd), -0.36(Cl)	0.67	Donor-acceptor
4	0.08	0.23	0.94	-0.27	0.81	0.05	+0.62(Pd), -0.36(Cl)	0.73	Donor-acceptor
5	0.08	0.23	0.95	-0.27	0.79	0.06	+0.62(Pd), -0.35(Cl)	0.73	Donor-acceptor

6.3.2. Monocations

$[Pd_3Cl_3(CH_3CN)_2(H_2O)]^+$ (iso1), ZORA-M06-L/triple-ζ*

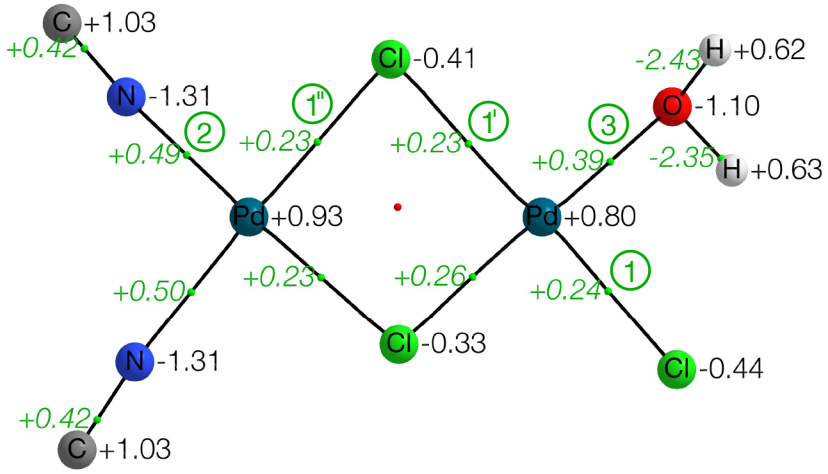

Bond	ρ_b	$\nabla^2\rho_b$	$\frac{G(r_b)}{\rho_b}$	$\frac{h_e(r_b)}{\rho_b}$	$\delta(A,B)$	ε_b	$q(A)$,$q(B)$	$\oint_{A\cap B}\rho(r_b)$	Bond type
1	0.10	0.24	0.92	-0.32	0.97	0.04	+0.80(Pd), -0.44(Cl)	0.86	Strong donor-acceptor
1'	0.06	0.23	1.07	-0.19	0.61	0.07	+0.80(Pd), -0.41(Cl)	0.57	Donor-acceptor
1''	0.08	0.23	0.97	-0.27	0.79	0.06	+0.93(Pd), -0.41(Cl)	0.69	Donor-acceptor
2	0.10	0.49	1.46	-0.24	0.65	0.12	+0.93(Pd), -1.31(N)	0.73	Donor-acceptor
3	0.07	0.39	1.44	-0.15	0.51	0.11	+0.80(Pd), -1.10(O)	0.63	Donor-acceptor

* CH_3 groups were omitted for clarity; see the main text for the whole optimized structure.

$[Pd_3Cl_3(CH_3CN)_2(H_2O)]^+$ (iso1), ZORA-TPSS/triple-ζ*

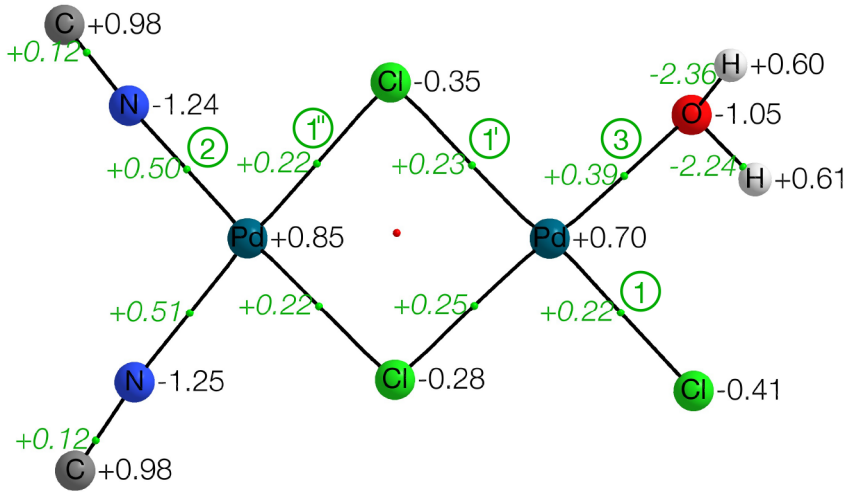

Bond	ρ_b	$\nabla^2\rho_b$	$\frac{G(r_b)}{\rho_b}$	$\frac{h_e(r_b)}{\rho_b}$	$\delta(A,B)$	ε_b	$q(A)$,$q(B)$	$\oint_{A\cap B}\rho(r_b)$	Bond type
1	0.10	0.22	0.89	-0.33	0.99	0.04	+0.70(Pd), -0.41(Cl)	0.89	Strong donor-acceptor
1'	0.07	0.23	1.02	-0.23	0.67	0.06	+0.70(Pd), -0.35(Cl)	0.62	Donor-acceptor
1''	0.09	0.22	0.92	-0.29	0.82	0.05	+0.85(Pd), -0.35(Cl)	0.72	Donor-acceptor
2	0.11	0.50	1.43	-0.28	0.71	0.10	+0.85(Pd), -1.24(N)	0.79	Donor-acceptor
3	0.08	0.39	1.38	-0.19	0.57	0.10	+0.70(Pd), -1.05(O)	0.69	Donor-acceptor

* CH_3 groups were omitted for clarity; see the main text for the whole optimized structure.

$[Pd_3Cl_3(CH_3CN)_2(N_2)]^+$ (iso1), ZORA-M06-L/triple-ζ*

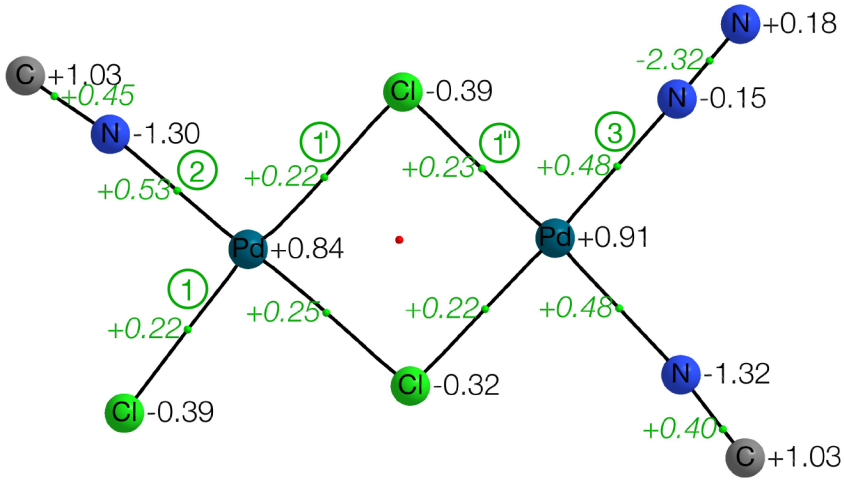

Bond	ρ_b	$\nabla^2\rho_b$	$\frac{G(r_b)}{\rho_b}$	$\frac{h_e(r_b)}{\rho_b}$	$\delta(A,B)$	ε_b	$q(A)$,$q(B)$	$\oint_{A\cap B}\rho(r_b)$	Bond type
1	0.10	0.22	0.89	-0.32	1.00	0.02	+0.84(Pd), -0.39(Cl)	0.83	Strong donor-acceptor
1'	0.06	0.22	1.07	-0.18	0.58	0.01	+0.84(Pd), -0.39(Cl)	0.55	Donor-acceptor
1''	0.08	0.23	0.95	-0.28	0.81	0.04	+0.91(Pd), -0.39(Cl)	0.69	Donor-acceptor
2	0.11	0.53	1.47	-0.26	0.70	0.12	+0.84(Pd), -1.30(N)	0.77	Donor-acceptor
3	0.09	0.48	1.55	-0.19	0.57	0.13	+0.91(Pd), -0.15(N)	0.72	Donor-acceptor

* CH_3 groups were omitted for clarity; see the main text for the whole optimized structure.

$[Pd_3Cl_3(CH_3CN)_2(N_2)]^+$ (iso1), ZORA-TPSS/triple-ζ*

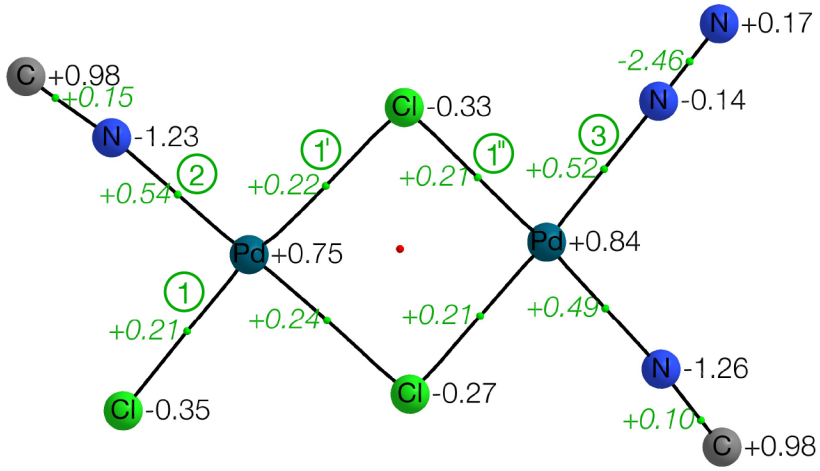

Bond	ρ_b	$\nabla^2\rho_b$	$\frac{G(r_b)}{\rho_b}$	$\frac{h_e(r_b)}{\rho_b}$	$\delta(A,B)$	ε_b	$q(A)$,$q(B)$	$\oint_{A\cap B}\rho(r_b)$	Bond type
1	0.10	0.21	0.86	-0.33	1.02	0.01	+0.75(Pd), -0.35(Cl)	0.85	Strong donor-acceptor
1'	0.07	0.22	1.02	-0.22	0.65	0.01	+0.75(Pd), -0.33(Cl)	0.61	Donor-acceptor
1''	0.09	0.21	0.90	-0.30	0.84	0.03	+0.84(Pd), -0.33(Cl)	0.72	Donor-acceptor
2	0.12	0.54	1.44	-0.30	0.76	0.10	+0.75(Pd), -1.23(N)	0.83	Donor-acceptor
3	0.10	0.52	1.52	-0.26	0.66	0.11	+0.84(Pd), -0.14(N)	0.74	Donor-acceptor

* CH_3 groups were omitted for clarity; see the main text for the whole optimized structure.

7. References

1 D. Dutta and T. Chen, *Bioinformatics*, 2007, **23**, 612–618.

2 M. K. Łacki, M. Startek, D. Valkenborg and A. Gambin, *Anal. Chem.*, 2017, **89**, 3272–3277.

3 M. K. Łącki, D. Valkenborg and M. P. Startek, *Anal. Chem.*, 2020, **92**, 9472–9475.

4 I. M. Park, S. Seth, A. R. C. Paiva, L. Li and J. C. Principe, *IEEE Signal Process. Mag.*, 2013, **30**, 149–160.

5 A. R. C. Paiva, I. Park and J. C. Príncipe, *Neural Comput.*, 2009, **21**, 424–449.

6 A. G. Brenton and A. R. Godfrey, *J. Am. Soc. Mass Spectrom.*, 2010, **21**, 1821–1835.

7 C. Bannwarth, E. Caldeweyher, S. Ehlert, A. Hansen, P. Pracht, J. Seibert, S. Spicher and S. Grimme, *Wiley Interdiscip. Rev. Comput. Mol. Sci.*, 2021, **11**, e1493.

8 S. Grimme, *J. Chem. Theory Comput.*, 2019, **15**, 2847–2862.

9 C. Bannwarth, S. Ehlert and S. Grimme, *J. Chem. Theory Comput.*, 2019, **15**, 1652–1671.

10 F. Neese, *Wiley Interdiscip. Rev. Comput. Mol. Sci.*, 2012, **2**, 73–78.

11 P. Pracht, F. Bohle and S. Grimme, *Phys. Chem. Chem. Phys.*, 2020, **22**, 7169–7192.

12 N. C. Handy and A. J. Cohen, *Mol. Phys.*, 2009, **99**, 403–412.

13 C. Lee, W. Yang and R. G. Parr, *Phys. Rev. B*, 1988, **37**, 785–789.

14 S. Grimme, J. Antony, S. Ehrlich and H. Krieg, *J. Chem. Phys.*, 2010, **132**, 154104.

15 S. Grimme, S. Ehrlich and L. Goerigk, *J. Comput. Chem.*, 2011, **32**, 1456–1465.

16 J. Zheng, X. Xu and D. G. Truhlar, *Theor. Chem. Acc.*, 2011, **128**, 295–305.

17 E. J. Baerends, D. E. Ellis and P. Ros, *Chem. Phys.*, 1973, **2**, 41–51.

18 B. I. Dunlap, J. W. D. Connolly and J. R. Sabin, *J. Chem. Phys.*, 1979, **71**, 3396.

19 C. Van Alsenoy, *J. Comput. Chem.*, 1988, **9**, 620–626.

20 R. A. Kendall and H. A. Früchtl, *Theor. Chim. Acta*, 1997, **97**, 158–163.

21 K. Eichkorn, F. Weigend, O. Treutler and R. Ahlrichs, *Theor. Chim. Acta*, 1997, **97**, 119–124.

22 K. Eichkorn, O. Treutler, H. Öhm, M. Häser and R. Ahlrichs, *Chem. Phys. Lett.*, 1995, **240**, 283–289.

23 J. L. Whitten, *J. Chem. Phys.*, 1973, **58**, 4496.

24 F. Weigend, *Phys. Chem. Chem. Phys.*, 2006, **8**, 1057.

25 E. van Lenthe, E. J. Baerends and J. G. Snijders, *J. Chem. Phys.*, 1993, **99**, 4597–4610.

26 C. van Wüllen, *J. Chem. Phys.*, 1998, **109**, 392.

27 Y. Zhao and D. G. Truhlar, *J. Chem. Phys.*, 2006, **125**, 194101.

28 J. Tao, J. P. Perdew, V. N. Staroverov and G. E. Scuseria, *Phys. Rev. Lett.*, 2003, **91**, 146401.

29 F. Weigend and R. Ahlrichs, *Phys. Chem. Chem. Phys.*, 2005, **7**, 3297.

30 D. A. Pantazis, X.-Y. Chen, C. R. Landis and F. Neese, *J. Chem. Theory Comput.*, 2008, **4**, 908–919.

31 AIMAll (Version 19.10.12), Todd A. Keith, TK Gristmill Software, Overland Park KS, USA, 2019 (aim.tkgristmill.com).

32 M. D. Hanwell, D. E. Curtis, D. C. Lonie, T. Vandermeerschd, E. Zurek and G. R. Hutchison, *J. Cheminform.*, 2012, **4**, 17.

33 Persistence of Vision Pty. Ltd. (2004), Persistence of Vision Raytracer (Version 3.7) [Computer software]. Retrieved from http://www.povray.org/.

34 A. Herráez, *Biochem. Mol. Biol. Educ.*, 2006, **34**, 255–261.